A FIRST PRINCIPLES MODEL AND NUMERIC SOLUTION METHODS FOR A SYSTEM OF SELF-ORGANIZING CONDUCTORS

BY

CORY STEPHENSON

DISSERTATION

Submitted in partial fulfillment of the requirements
for the degree of Doctor of Philosophy in Physics
in the Graduate College of the
University of Illinois at Urbana-Champaign, 2018

Urbana, Illinois

Doctoral Committee:

Professor Alexey Bezryadin, Chair
Professor Alfred W. Hübler, Director of Research
Professor Karin A. Dahmen
Professor Matthias Grosse Perdekamp
Professor Richard Weaver

Abstract

Electrical networks have long been studied in the context of non-equilibrium thermodynamics, particularly in the linear regime, due to both their theoretical convenience and their experimental accessibility. Of more recent interest is the behaviour of self-organizing electrical networks which necessarily exist in the non-linear regime where several proposed non-equilibrium thermodynamic principles are conjectured to apply. However, extension of conventional electrical network models to this regime is challenging due to the requirement that the topology of the network be dynamic. Additionally, the system dynamics must be modelled in a way that retains the essential physics while still being numerically solvable. In this work, we develop a first-principles model of a system of electrically conducting particles which self-organizes to form complex electrical networks. The resulting model contains many non-linear interactions between the constituents, and so we develop the methods necessary to numerically integrate the equations of motion efficiently. This leads to a new method of numerically calculating the forces between conducting objects in a dynamic configuration. We then use these methods to reproduce experimental results regarding the network topology, and find that our model is in agreement with experiment. Interestingly, we observe that the model predicts various measures of the network topology remain constant during the self-organization process. These developments may be applied in further exploration of principles regarding energy dissipation and entropy production in electrical networks beyond the linear regime, as a physical model of the process as well as the methods of numerical solution has been developed and validated with comparison to experiment.

To my parents, Susan and Jerry, to my wife Yewon, and to Alfred W. Hübler

Acknowledgments

First and foremost, I want to thank Professor Alfred W. Hübler, my advisor and collaborator through all of this work. I was fortunate to learn so much from him over the years. I will not forget his unique insight, and I will always remember to ramp up the voltage if I want to make things interesting. Special thanks also go to Professor Karin A. Dahmen, who provided input and advice at a crucial time. Her guidance in the final stages of the process was invaluable. Thank you also to Professor Bezryadin, both for the experimental work that informed my thinking on this system. Thank you to Professor Richard Weaver for his helpful comments on this document. Thank you also to Professor Mattias Perdekamp for his interesting ideas on broader applications of this work.

I would also like to thank the UIUC Physics department as a whole for it's hospitality over the years. In particular, I want to personally thank Professor Cooper for all the work he has done for all the graduate students in the department, including myself in particular. Thank you also to Mrs. W. R. Wimmer, who has been extremely helpful in all circumstances. I met many of the most intelligent and kindest people I will ever know at the University of Illinois. Thank you all for the many fascinating discussions.

Of course, none of this would have been possible without my parents Susan and Jerry Stephenson who always supported me even when it wasn't easy. They encouraged my interest in physics even before I was old enough to remember.

Finally, I cannot give enough thanks to my wife Yewon Gim, who I met during my time at UIUC. We shared many of the difficulties of the graduate school experience together, and it is safe to say I wouldn't have made it through without her. She brings out the best in me.

This work was partially supported by US Air Force Grant: FA9453-14-1-0247, Office of Naval Research Grants: N00014-14-1-0381 and N00014-15-1-2397, US Army Contract W9132T-14-A-0001 (Dr. Marsh, CERL) and DOE HRL Subcontract 9060-000706-DS UIUC

Academic Disclaimer: The author wrote this dissertation in support of requirements for the degree Doctor of Philosophy in Physics at University of Illinois, Urbana-Champaign.

Table of Contents

List of Figures

Chapter 1

Introduction

Self-organization and pattern formation is found nearly everywhere in nature. In spite of this, general principles describing the process remain elusive. Central to this is the difficulty of deducing the emergent behaviour of non-linear systems containing many interacting components, even if the interactions follow known dynamical laws. Due to the inherent complexity of natural systems which exhibit self-organization, first principles models often become intractable as the number of interacting objects grows. As a consequence, little is known about the physical principles that link the aggregate properties of self-organizing systems with familiar thermodynamic quantities such as entropy production and power dissipation. These quantities are expected to be important, as a defining characteristic of these systems is a trade-off between the energy input and dissipation which stabilizes the stationary state.

This work is focused on the creation of a numerically solvable model of a specific type of self-organizing system consisting of a number of mobile conducting objects in an insulating fluid. This type system is known to exhibit self-organization in two different scenarios. In the first scenario, a constant electrical potential difference is maintained between two electrodes. Conducting particles suspended in the fluid the self-organize to form wire-like connections between the two electrodes and the total resistance of the system drops. This effect is known to occur in a wide range of experimental parameters. It has been observed in systems of carbon nanoparticles[4] and nanotubes[2] suspended in toluene, as well as ball bearings in castor oil [5, 6].

In the second scenario, electrical charge is sprayed onto the particles via field emission from the sharp tip of an electrode suspended above the setup. The particles then self-

organize to form dendritic structures to transport the excess charge to a sink electrode held at ground potential [1, 3, 7]. The resulting structures are quite complex, as can be seen in Fig. 1.1, which shows the structure at various stages during the formation process.

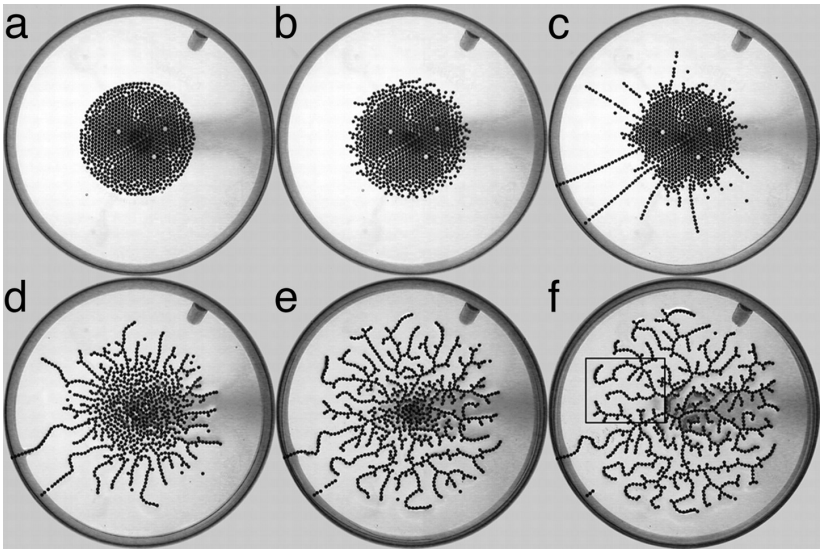

Figure 1.1: Formation of treelike structure in a system of conducting particles in castor oil over time when charge is sprayed from above. Figure taken from [1].

It is this second scenario that the rest of this work will be focused on, however many of the techniques developed are also suitable to modelling the first scenario as well. This document is laid out as follows:

Chapter 2 contains a high level overview of some of the general variational principles proposed in the context of non-equilibrium systems. This chapter serves to summarize the connection between the detailed interactions of the individual system components and the large scale thermodynamic quantities such as entropy production which is directly relevant to the conventional understanding of self-organization. It begins with a discussion of the role played by the maximum entropy principle in equilibrium thermodynamics in Sec. 2.2, and how it relates to other well known principles such as the principle of minimum free energy. Prigogine's minimum entropy production principle for non-equilibrium stationary states near equilibrium is then discussed in the linear regime near equilibrium in Sec. 2.3. Finally, the more speculative maximum entropy production principle is described in Sec.

2.4, along with the relationship between this principle and Prigogine's principle.

Chapter 3 motivates the study of dynamic electric networks as a good system to study self-organizational phenomena, and briefly overviews some of the relevant previous results found in the literature for this type of system. Section 3.1 outlines a well known principle of minimal power dissipation in systems with static resistivity, and what is required in order to observe more complex phenomena. Section 3.2.1 re-derives a minimum resistance principle for the self-organizing conductor system which holds in special circumstances. Section 3.2.2 briefly discusses some recent evidence for the maximum entropy production principle as it applies to a system of self organizing carbon nanotubes suspended in toluene. Section 3.2.3 introduces some results involving the topological properties of the treelike structures formed by conducting particles when charge is added via field emission at a constant rate.

Chapter 4 discusses some of the experimental work carried out and how it informs the relevant effects that must be included in the model. Section 4.2 contains theoretical and experimental results regarding the mechanism by which a single conducting modifies the electrical resistance of a region of insulating fluid by shuttling charge between high and low electric potentials. Section 4.3 contains theoretical and experimental results aimed at clarifying the multi-conductor interactions that lead to local stability of the self-organized structure.

Chapter 5 specifies the full form of the self-organizing wire network model. Some of the key assumptions of the model are outlined in Sec. 5.2. The dynamics of the electrical degrees of freedom is specified in Sec. 5.3, while the dynamics of the mechanical degrees of freedom can be found in Sec. 5.4. The full form of the model can be seen in Sec. 5.5, along with the initial conditions necessary for solving the forward problem.

Chapter 6 develops the numerical methods used to solve the model in a practical manner. This is somewhat involved for this model, and so this chapter begins with a brief summary of the computational framework that makes the solution possible in Sec. 6.2. From there, Sec. 6.3 develops the methods used to solve for the electrical potential in the regions between

conductors, along with the boundary conditions that must be used to do so. This requires the evaluation of several surface integrals, and the method used to do this can be found in Sec. 6.4. It turns out that computation of the electrostatic boundary conditions for this system is difficult, and so Sec. 6.5 provides a method to do this efficiently, along with both a proof that this method finds the correct solution and some benchmarks on a simple test problem. Finally, Sec. 6.6 deals with some practical issues with handling the collisions between conductors, and the equations of motion are integrated in Sec. 6.7.

Chapter 7 presents the analysis methods and some of the results obtained from the model, and how they compare to those obtained from experiments. Section 7.2 defines how a collection of particle positions is turned into both an undirected and directed graph for later analysis. Section 7.3 calculates the degree distribution from this graph from the fraction of branch points and endpoints it contains with the use of some geometric constraints. Section 7.4 compares the degree distribution calculated from the model to the experimentally observed values and finds an exact match. Additionally, Sec. 7.5 compares the Strahler number distribution calculated with the model to the experimental values and likewise finds agreement. Surprisingly, this model suggests that these topological quantities are constant throughout the self-organizational process.

Chapter 8 concludes the document with a summary of the results obtained in this work and discusses avenues of continuation.

Chapter 2

Variational principles in non-equilibrium thermodynamics

The emergence of macroscopic order from microscopic physics is a challenging problem in thermodynamics. In equilibrium, great success has been had in applying variational methods, notably the maximization of entropy and the minimization of free energy, to determine the relationships between observed macroscopic variables. However, in the non-equilibrium case, the problem is much more difficult, and significant progress has only truly been made in the linear near-equilibrium approximation. Beyond this, some conjectures, notably the maximum entropy production principle, attempt to make statements that can be extended to the non-linear regime. By nature, experiments probing the far from equilibrium behaviour of complex systems is challenging, and so the veracity or domain of applicability of these far from equilibrium conjectures remains cloudy. It is the goal of this chapter to present the roles and relationships between the various in equilibrium and out of equilibrium variational principles in thermodynamics, and motivate dynamic electrical networks as a conceptually clear testbed for non-equilibrium ideas.

2.1 The under-determined problem

The problem of thermodynamics is fundamentally an under-determined one. Given the large number of microscopic degrees of freedom present in a typical macroscopic system, there is certainly not enough information contained in the knowledge of the macroscopic state to sufficiently constrain the microscopic state. Put another way, there are typically many microscopic states which are compatible with a given macrostate. The relationship

between the macroscopic variables is determined by how the set of compatible microstates changes with the macroscopic variables. In this context, the role of a variational principle is to constrain the possible relationships between macroscopic variables. If such a principle exists for the system in question, it may be possible to obtain useful results from the macroscopic constraints without explicit knowledge of the microscopic state. In the typical (equilibrium) case, the variational principle is the principle of maximum entropy. This principle is especially powerful in that it gives rise to a non-trivial probability distribution over the microstates in terms of the macroscopic constraints, and so allows calculation of many ensemble averaged quantities, as well as relationships between macroscopic variables.

However, the non-equilibrium case is less understood. For linear systems or systems near equilibrium, there are known principles which may be applied, notably Prigogine's principle of minimum entropy production. This principle constrains the possible stationary states of a linear non-equilibrium system to those in which the entopy production is at a local minimum in which any infinitesimal departure from the state is associated with an increase in the total entropy production subject to external constraints. However, for nonlinear (far from equilibrium) systems the general principles are unknown if they exist at all. One conjectured principle, that of maximum entropy production, has been extensively studied, although consensus has not yet been reached as to its validity. This principle aims to constrain the possible relationships between generalized thermodynamic variables (called fluxes and flows) to the set of those relationships that maximize the entropy production. The power of these two non-equilibrium principles is certainly less than the maximum entropy principle, however they both provide useful constrains on the relationships between the macroscopic variables.

2.2 Entropy maximization in equilibrium

In the context of statistical mechanics, the connection between the thermodynamic variables and the microscopic variables in equilibrium is obtained by maximizing the Gibbs entropy with respect to the macroscopic constraints[8]. Even though the number of microscopic degrees of freedom may be many orders of magnitude larger than the number of macroscopic constraints, this procedure allows the calculation of a probability distribution over the microscopic degrees of freedom from which meaningful (and physically correct) information about the macroscopic state of the system can be derived. As an example, consider a system consisting of N non-interacting point particles confined to a $3D$ volume V. In principle, there are a total of $6N$ degrees of freedom, which for a single mol ($N \sim 6 \times 10^{23}$) is astronomically large. However, the presence of a single macroscopic constraint in the form of a fixed temperature T (related to the mean total energy E by the Boltzmann constant k_b and the relation $\langle E \rangle = k_B T$) of the gas is enough to allow calculation of a variety of other thermodynamic quantities. Following the principle of maximum entropy, a probability distribution $p(\{x\},\{p\}) \equiv p(\{x_1, x_2, .., x_N\}, \{p_1, p_2, ..., p_N\})$ over the microscopic degrees of freedom is assumed. This distribution is chosen such that the entropy functional

$$S\left[p(\{x\},\{p\})\right] = -k_B \int_\Omega p(\{x\},\{p\}) \ln\left(p(\{x\},\{p\})\right) \tag{2.1}$$

is maximized subject to the constraint

$$\langle E \rangle = \int_\Omega E\left(\{x\},\{p\}\right) p(\{x\},\{p\}) \equiv k_B T \tag{2.2}$$

Here the integrals are taken over the allowed values of the microscopic degrees of freedom, which in this case correspond to x inside volume V and any p. A theorem due to Boltzmann states that given M constraints on expectation values of functions of the microscopic degrees of freedom $\langle f_i\left(\{x\},\{p\}\right)\rangle = a_i$ for $i = 1, 2, ..., M$, the probability distribution over the

microscopic degrees of freedom which maximizes the entropy of Equation 2.1 is given by

$$p(\{x\},\{p\}) = \mathcal{Z}^{-1} \exp\left[\sum_{i=1}^{M} \lambda_i f_i\left(\{x\},\{p\}\right)\right] \tag{2.3}$$

Where $\mathcal{Z}$ is the partition function, and the values of the λ_i's are chosen to satisfy the constraints. For the specific case of fixed temperature, this gives

$$p(\{x\},\{p\}) = \mathcal{Z}^{-1}\left(N,V,T\right) \exp\left[-\frac{1}{k_B T} E\left(\{x\},\{p\}\right)\right] \tag{2.4}$$

From this, the expectation value of any macroscopic observable (which is in general a function of the microscopic degrees of freedom) may be calculated. Furthermore, this example generalized beyond a single fixed temperature constraint. The success of the theory[9] stems from the fact that many relevant quantities can be related to the partition function, which is a function of macroscopic variables only. In spite of the high number of degrees of freedom and potentially complex dynamics of the underlying physical system, if a suitable set of constraints can be found and the partition function can be calculated, a coherent macroscopic theory emerges.

2.2.1 Relationship to the thermodynamic potentials

While the entropy maximization procedure leads to the partition function, the classical thermodynamic potentials can also be obtained from this principle. In equilibrium, the entropy (abbreviated as S) can be calculated as

$$\begin{aligned} S &= -k_B \int_\Omega p(\{x\},\{p\}) \ln\left(p(\{x\},\{p\})\right) \\ &= -k_B \int_\Omega p(\{x\},\{p\}) \ln\left(\mathcal{Z}^{-1} \exp\left[\sum_{i=1}^{M} \lambda_i f_i\left(\{x\},\{p\}\right)\right]\right) \end{aligned} \tag{2.5}$$

for the general case. Continuing the calculation gives

$$\begin{aligned} S &= -k_B \int_\Omega p(\{x\},\{p\}) \left[\sum_{i=1}^{M} \lambda_i f_i(\{x\},\{p\}) - \ln(\mathcal{Z}) \right] \\ &= -k_B \sum_{i=1}^{M} \lambda_i \langle f_i(\{x\},\{p\}) \rangle + k_B \ln(\mathcal{Z}) \end{aligned} \tag{2.6}$$

Assuming the constraint on the mean energy is present in the general case, and writing $\langle f_i(\{x\},\{p\}) \rangle = Y_i$, $\lambda_i = X_i$ for the rest of the constraints, this becomes

$$S = \frac{\langle E \rangle}{T} - \sum_{i=2}^{M} X_i Y_i + k_B \ln(\mathcal{Z}) \tag{2.7}$$

Making the definition $-k_B T \ln(\mathcal{Z}) = F$ for the free energy F and redefining $X_i \to T X_i$, this becomes

$$F = \langle E \rangle - TS + \sum_{i=2}^{M} X_i Y_i \tag{2.8}$$

Which is the familiar expression for the free energy for generalized intensive, extensive variables X,Y. Note the maximization of S with the fixed constraint implies F should be minimized.

2.2.2 Relationship to information theory

The principle of maximum entropy can be related to a type of statistical inference in which the information about the microstate of the system is minimized subject to the macroscopic constraints[10, 11]. From this view, the expression for entropy in Eq. 2.1 is essentially the continuous version of the Shannon information[12]. Following Shannon, the information required to specify the state of a system which can be in one of N states is given by

$$S_I = -\sum_{i=1}^{N} p_i \ln p_i \tag{2.9}$$

where p_i is the probability of finding the system in the i^{th} state. This quantity is called the information entropy. The principle of maximum entropy can thus be interpreted as a statement that in the absence of any extra information, the probability distribution over the microstates should be the one that contains only the information contained in the macroscopic constraints. This correspondence is exact (up to the constant k_B) in the case of a discrete distribution over the microstates.

2.2.3 Out of equilibrium

Unfortunately, this procedure does not generalize to non-equilibrium states. In the simple case under consideration, if the fixed temperature of the system is changed from an initial value T_1 to some new value of T_2, by changing the temperature of the boundaries for example, the system will take some time to reach a new equilibrium at this temperature. During this time, different regions of the system will have different temperatures, and the dynamics of the temperature profile will depend on the microscopic dynamics of the system. Therefore, in the intermediate states, temperature can no longer be used as a global constraint as in Eq. 2.2, and the entropy maximization procedure as currently stated cannot be performed.

This problem does not only concern the time dependent relaxation to equilibrium. The same issues can arise in stationary states as well. If, for example, some parts of the system boundaries are held at temperature T_1 and others are held at temperature T_2, even if the system reaches a stationary state in which different regions have different but unchanging temperatures, it is still unclear how to calculate the resultant temperature profile or carry out the entropy maximization procedure. This is an example of a non-equilibrium stationary state.

2.3 Near-equilibrium states

The maximum entropy principle of section 2.2 can be extended to make meaningful statements about states which are near equilibrium[13]. Without loss of generality, let $a_1, a_2, ..., a_N$ be a set of some variables which describe the system and are zero in equilibrium. Concrete examples of this type of variable include excess temperature, or excess pressure from equilibrium. The entropy can then be expanded about equilibrium as

$$S = S_{eq} - \frac{1}{2}\sum_{i,j=1}^{N} G_{ij} a_i a_j + \mathcal{O}\left(a^4\right) \tag{2.10}$$

For states sufficiently close to equilibrium, the higher order terms may be dropped. Here, the matrix given by the elements G_{ij} is positive definite, and also symmetric ($G = G^T$, owing to the expansion about equilibrium), which follows from the requirement that the entropy is maximized when all the a's are zero. Following Prigogine[14], the generalized forces X_i (called such as they follow the negative gradient of the entropy) can be introduced in terms of G and the variables a.

$$X_i \equiv -\frac{\partial S}{\partial a_i} = -\sum_{j=1}^{N} G_{ij} a_j \tag{2.11}$$

These are assumed to depend only on the same variables as in the nearby equilibrium, and can be related to the thermodynamic forces in section 2.2.1. The rate of change of the entropy $\dot{S}$, also called the entropy production σ, is then

$$\dot{S} \equiv \sigma = -\sum_{i,j=1}^{N} G_{ij} \dot{a}_i a_j = \sum_{i=1}^{N} \dot{a}_i X_i \tag{2.12}$$

The quantities $J_i \equiv \dot{a}_i$ are the fluxes which act to drive the system back to equilibrium. In terms of these, the entropy production is

$$\sigma = \sum_{i=1}^{N} J_i X_i \tag{2.13}$$

In principle, the fluxes will depend on the non-equilibrium state (which is determined by the a_i's or equivalently the X_i's) according to some unknown relationship $J_i = J_i(X_1, X_2, ..., X_N)$. In equilibrium, the fluxes vanish, and so in the near equilibrium regime these can be expanded as

$$J_i = \sum_{j=N}^{N} L_{ij} X_j + \mathcal{O}\left(X^2\right) \tag{2.14}$$

with some linear coefficients L_{ij}. This gives the entropy production entirely in terms of the forces.

$$\sigma = \sum_{ij=N}^{N} L_{ij} X_i X_j \tag{2.15}$$

The second law of thermodynamics requires that the entropy production be positive for all states near equilibrium, and zero in the equilibrium state. This implies that the matrix given by the elements L_{ij} is positive definite, and also symmetric following the same argument as for G. Thus, there exists the relationships

$$L_{ij} = L_{ji} \tag{2.16}$$

Which are known as the Onsager reciprocal relations[15, 16]. These relations describe certain well known near-equilibrium phenomena, such as the various thermoelectric effects in which they manifest as relationships between the temperature gradient, electric potential gradient, and the flows of charge and heat[17].

While the above treatment was carried out for near equilibrium states in which the macroscopic variables are constant in the region of interest, the generalization to systems in which the macroscopic variables vary over the region of interest is straightforward. In this scenario, the system can be subdivided into infinitesimal regions in which the macroscopic variables are constant, and conserved quantities such as energy, mass, and charge are governed by continuity equations. In addition to the usual conservation laws, the entropy also obeys a continuity equation, with a source term corresponding to the entropy production at

a given location. This is the basis of classical irreversible thermodynamics[18].

2.3.1 Prigogine's Minimum Entropy Production principle

In the region near equilibrium where the linear approximations hold, the relaxation to equilibrium is governed by a system of linear differential equations. Combining Eq. 2.11 and Eq. 2.14 gives the time evolution for the forces.

$$\dot{X}_i = -\sum_{j,k=1}^{N} G_{ij} L_{jk} X_k \tag{2.17}$$

This implies that the relaxation to equilibrium (the decay of the forces to zero) occurs monotonically. Furthermore, the entropy production is always decreasing in accordance with the equation

$$\dot{\sigma} = 2\sum_{i,j=1}^{N} L_{ij} X_i \dot{X}_j = -2\sum_{i,j,k,l,m=1}^{N} L_{ij} G_{kl} L_{lm} X_i X_m = -2X^T A X \tag{2.18}$$

Here A is a positive semi-definite matrix, as it is formed from the product of L and G which are also positive semi-definite, thus the rate of change of the entropy production is always negative. However, a non-equilibrium stationary state may be maintained by constraining the values that one or more of the forces (or fluxes) can take. The form of Eq. 2.18 shows that the entropy production will decrease as much as possible, until it achieves the minimum value permitted by the constraints. This is Prigogine's minimum entropy production principle, which can be proved more rigorously[19, 14, 20]. Phrased slightly differently, this principle states that the non-equilibrium stationary state has a lower entropy production than any transient states that obey the same constraints. Therefore, the entropy production is a Lyapunov function for the system in the linear regime.

This principle is one of the more well known examples of a variational principle for non-equilibrium states. Unfortunately, it only applies to states which are near enough to

equilibrium for the linear approximations to hold. This greatly limits its capability for describing general non-equilibrium phenomena.

2.4 Far from equilibrium states

Due to the success of non-equilibrium thermodynamics in the linear regime, there is a strong desire to extend the theory beyond the linear region near equilibrium. The fundamental difficulties is twofold. For one, there are no guarantees that the expansion in Eq. 2.10 can be written in terms of the same variables that are relevant in equilibrium. It could easily be the case that new variables are important in calculating the entropy far from equilibrium, but decay rapidly as equilibrium is approached. It is likely that these variables will depend in detail on the microscopic properties of the system under consideration. Secondly, even if it is assumed that the equilibrium variables are still the only ones that are needed, the assumption of Eq. 2.14 that the fluxes may be linearly related to the generalized forces is certainly violated. While it seems quite difficult to address the first difficulty in a thermodynamic framework, it is conceivable that the second may be fruitfully attacked.

One tempting avenue results from the observation that the dynamics given by the linear relationships between the forces and fluxes bears a resemblance to steepest ascent of the entropy. Instead of working with the entropy, the entropy production can itself be assumed to be a function of the generalized forces, and expanded about the equilibrium.

$$\dot{S} = \sigma = \sum_{i,j=1}^{N} L_{ij} X_i X_j + \mathcal{O}\left(X^3\right) \tag{2.19}$$

Since the entropy production must be zero in equilibrium, and cannot be negative near equilibrium if the equilibrium is stable, L_{ij} must again be a positive semidefinite matrix.

With this expansion, the gradient of the entropy production is given by

$$\frac{\partial \sigma}{\partial X_i} = \sum_{j=1}^{N} L_{ij} X_j \tag{2.20}$$

Which is recognized to be the fluxes of Eq. 2.14. At least in the linear regime, it appears as if the relationship $J_i = \frac{\partial \sigma}{\partial X_i}$ holds. Effectively the fluxes are oriented in the direction in which the entropy production increases at the largest rate. Taking the time derivative of the entropy production, the expansion also gives

$$\dot{\sigma} = 2 \sum_{i,j=1}^{N} L_{ij} \dot{X}_i X_j = 2 \sum_{i=1}^{N} J_i \dot{X}_i \tag{2.21}$$

This has the interpretation that changes in the thermodynamic forces are projected onto the direction of steepest ascent of the entropy production as described by the thermodynamic fluxes. This is due to the specific nature of the linear relationship between the forces and the fluxes.

2.4.1 Maximum entropy production principle

While the relationship between the fluxes, forces, and maximum rate of entropy production has only been motivated for the linear case, it is tempting to wonder if it can be extended to the non-linear case as well. A popular conjecture states that the observed relationship between the thermodynamic fluxes and forces is the one which gives the largest entropy production. This is the central idea behind the maximum entropy production principle, which has been proposed more or less independently in many different contexts and forms [21, 22, 20, 23] and reviewed thoroughly in [24]. While there are several conceptually similar forms, the least controversial[25] and most rigorously formulated is the principle as stated by Zeigler[22, 23]. This is the version of the principle discussed in this section.

With this principle in mind, the above motivation must be reinterpreted with a different

perspective. Even in the non-linear regime, the relationship between the entropy production and the forces and fluxes can be defined to obey the same relation as near equilibrium.

$$\sigma = \sum_{i=1}^{N} J_i X_i \tag{2.22}$$

In principle, the entropy production is related to the power dissipation of the system, and so it may be a known function of the fluxes and the forces even far from equilibrium. The maximum entropy production principle then asserts that the relationship between the fluxes and forces is the one which maximizes the entropy production subject to the constraint that Eq. 2.22 holds. Assuming fixed forces for simplicity (the principle works the same regardless of which variables are fixed) the maximization can be performed using the calculus of variations.

$$\begin{aligned} \delta_{J_i} \left(\sigma \left[\{J\} \right] - \lambda \left(\sigma \left[\{J\} \right] - \sum_{i=1}^{N} J_i \left(\{X\} \right) X_i \right) \right) \Bigg|_{\{X\},\lambda} &= 0 \\ \delta_{\lambda} \left(\sigma \left[\{J\} \right] - \lambda \left(\sigma \left[\{J\} \right] - \sum_{i=1}^{N} J_i \left(\{X\} \right) X_i \right) \right) \Bigg|_{\{J\},\{X\}} &= 0 \end{aligned} \tag{2.23}$$

Where λ is a Lagrange multiplier that enforces the relationship given by Eq. 2.22. The solution to these equations is conjectured to give the relationship between the fluxes and forces even far from equilibrium.

Using this principle alone, it is possible to reconstruct the reciprocal relations in the linear regime, which is not a trivial result, although it may appear so at first glance[25]. Here, it can be assumed that the entropy function is known to be given by the expansion about equilibrium:

$$\sigma = \sum_{i,j=1}^{N} L_{ij} X_i X_j \tag{2.24}$$

Here, L_{ij} is once again a positive semi-definite matrix. Without assuming the reciprocal relations, the fluxes may be related to the forces by an arbitrary invertible matrix M which

may not be symmetric. In general, the matrix M can be decomposed into a symmetric part H and a skew-symmetric part Ω, $M = H + \Omega$.

$$J_i = \sum_{j=1}^{N} H_{ij} X_j + \sum_{j=1}^{N} \Omega_{ij} X_j \tag{2.25}$$

Note that this does not violate the positivity of the entropy production, provided L is positive semi-definite, as the entropy production can now be written as

$$\sigma = \sum_{i=1}^{N} J_i X_i = \sum_{j=1}^{N} H_{ij} X_i X_j + \sum_{j=1}^{N} \Omega_{ij} X_i X_j \tag{2.26}$$

Here, the identification $L = H$ must hold if the entropy production is to be given by Eq. 2.24. The second term vanishes $\left(\sum_{j=1}^{N} \Omega_{ij} X_i X_j = 0\right)$ since Ω is skew-symmetric, and hence the entropy production remains positive. Using the relationship $X_i = \sum_{j=1}^{N} M_{ij}^{-1} J_j$, the partial derivative may be expressed as

$$\frac{\partial X_i}{\partial J_j} = M_{ij}^{-1} \tag{2.27}$$

Switching to the more illuminating matrix notation, $\frac{\partial X}{\partial J} = \left(M^T\right)^{-1}$ and $\sigma = X^T L X$, and $\sum_{i=1}^{N} J_i X_i = J^T X$. Thus, carrying out the derivatives of Eq. 2.23 gives the system of equations

$$\begin{aligned} 2(\lambda - 1) L \left(M^T\right)^{-1} X &= \lambda X \\ \sigma\left[\{J\}\right] &= J^T X \end{aligned} \tag{2.28}$$

Clearly, a solution is had when $\lambda = 2$ and $L\left(M^T\right)^{-1}$ is the identity matrix $\mathbb{I}$. Recalling $M = H + \Omega$ with $H = L$ along with the symmetry $L = L^T$ and antisymmetry $\Omega^T = -\Omega$, the solution is then given by

$$L\left(L - \Omega\right)^{-1} = \mathbb{I} \tag{2.29}$$

The only solution is $\Omega = 0$. Furthermore, it can be shown that this solution corresponds to

a maximum[25]. Therefore the linear relationships

$$J_i = \sum_{j=1}^{N} L_{ij} X_j \tag{2.30}$$

with $L = L^T$ are the ones which maximize the entropy production subject to the constraint $\sigma = \sum_{i=1}^{N} J_i X_i$. Thus, the Onsager reciprocal relations are generated by the known function for the entropy production and the assumption that the entropy production is maximized.

While this calculation was carried out assuming linearity, it can be extended to non-linear relationships as well, in which case the principle implies analogous symmetry relations in the coefficients of the higher order terms as well. Equation 2.23 is Zeigler's principle of maximum entropy production, and as the above derivation shows, it is non-trivially true in the linear regime near equilibrium. The validity of this principle in the non-linear regime is conjectured.

2.4.2 Relation to the minimum entropy production principle

Although the names of the two beyond equilibrium principles discussed above sound contradictory, they are actually compatible with one another. Prigogine's minimum entropy production principle states that given specific (linear) relations between the thermodynamic fluxes and forces, the entropy production of a given system is a Lyapunov function. That is, the total entropy production decreases until a stationary state, equilibrium or otherwise, is reached which is characterized by a minimum of the entropy production subject to any externally imposed constraints. This principle governs the dynamics of the system once the flux/force relationships have been specified. Zeigler's maximum entropy production principle on the other hand is a principle which selects the flux/force relationships on the basis that the entropy production is maximized subject to any constraints. There is then room for both principles to operate simultaneously as indeed they can be shown to do in the near equilibrium regime.

Chapter 3

Self-organization of resistor networks

Although Prigogine's minimum entropy production principle and the maximum entropy production principle can be shown to be valid in the linear regime near equilibrium, it is unclear how well either one generalizes to the nonlinear regime. Part of the difficulty is that it can be shown that neither principle completely generalizes in the mathematical sense [14, 25], but still, many physical systems appear to obey them[24, 21]. One particular challenge in determining the domain of validity of variational principles far from equilibrium is constructing experimental systems in which the high level principles can be studied at the same time as the fundamental microscopic physics. Without the understanding of both the macroscopic and microscopic physics of the test system, it is difficult to determine the properties which ultimately give rise to the macroscopic principles.

In the past, electrical networks have provided a natural test bed for a variety of non-equilibrium concepts. The stationary states of an electrical network is clearly related to the electric potential difference and flow of currents through network connections. The potentials and currents can be easily related to the generalized thermodynamic forces and flows respectively, and the entropy production can be related to the total power dissipation due to Joule heating. In addition, more complex relationships between these variables can also occur, such as in the thermoelectric effect. Therefore, this type of system fits easily into the thermodynamic framework. Furthermore, the stationary state of an electrical network can be modified by different constraints, notably either the presence of a current supply, or a fixed potential gradient between two or more components. While the most common electrical networks are linear, due to the linearity of Ohm's law, non-linearities may be introduced by

the addition of non-linear resistors.

3.1 Minimum power dissipation

Due to both their experimental and theoretical convenience, the thermodynamics of electrical networks has been well studied, with a few notable results. The oldest of which is due to Kirchhoff[26, 13] who first noticed a variational principle at work in the distribution of charge in a conductive material. In a material with conductivity σ, the stationary state of the electric potential is such that the total power dissipated by Joule heating is minimized. Using Ohm's law for the current density $\vec{J}$ and the electric potential or field ϕ or $\vec{E}$, $\vec{J} = \sigma\vec{E} = -\sigma\nabla\phi$, the power P dissipated in a volume V is

$$P = \int \left(\vec{J} \cdot \vec{E}\right) dV = \int \sigma \left(\nabla\phi\right)^2 dV \tag{3.1}$$

The stationary state configuration of the electric potential (or equivalently the current densities) is then the one that minimizes this integral given some boundary conditions. If the temperature is uniform, the expression for the power is related to the total entropy production of the system, and so Prigogine's minimum entropy production principle is satisfied. However, in this system, there is a more fundamental principle that causes the power dissipation to be minimized. The minima of equation 3.1 are determined by conservation of charge and the requirement that the system be stationary. From the continuity equation for charge Q

$$\frac{\partial Q}{\partial t} + \nabla \cdot \vec{J} = \frac{\partial Q}{\partial t} - \nabla \cdot \sigma\nabla\phi = 0 \tag{3.2}$$

If the system is stationary, the equation $\nabla \cdot \nabla\phi = 0$, and these solutions correspond to the minima of the total power dissipation in Eq. 3.1. In the uniform temperature case, the principle of minimum entropy production then naturally arises as a consequence of the more fundamental law of charge conservation.

3.1.1 Properties of a good test system

More complicated systems can be constructed by connecting N conducting nodes together with resistors. Let R_{ij} be the resistance between node i and j, and let each node have a different temperature T_i. Such a network can be thought of as a mathematical graph with the resistance matrix R_{ij} defining the connection weights. If some of the nodes are held at a fixed potential, or if there is current supplied to them, the unconstrained currents and potentials of the network will then distribute themselves such that a stationary state is reached. As stated, the stationary state is completely determined by conservation of energy and conservation of charge in the form of Kirchhoff's circuit laws for the current and potential. Only by allowing the resistances R_{ij} to also be variables which evolve according to some possibly non-linear dynamics does the system becomes complex enough to allow description in terms of the two principles for the entropy production discussed above. This implies that a good test system not only allows the electrical and thermal degrees of freedom to evolve, but the connectivity of the network must be dynamic as well. Unfortunately, electrical networks with a dynamic connectivity are quite difficult to model, and as a consequence no first-principles models exist. In addition, only a few theoretical results exist. Experimental results are more common, but are still relatively few in number.

3.2 Previous results in electrical networks

In spite of the difficult nature of the problem, a small number of relevant results do exist in the literature. Notably, a minimum total resistance theorem was proved[5] granted some rather restrictive and perhaps unphysical assumptions. On the experimental side, some results exist exploring the steady state topology of physically evolving electrical networks[1, 3]. Relatively recent results provide evidence that the steady state of the system is in fact governed by the maximum entropy production principle of section 2.4.1, which manifests as a maximization of electrical power dissipation. This section will review a few of the most notable results.

3.2.1 Principle of minimum resistance

Perhaps the most directly relevant theoretical result is the principle of minimum resistance for self-assembling electrical networks[5]. This principle is derived for the special case of spherical conductors of radius R in 2D interacting electrically through a dielectric medium. The principle states that the resistance between the pair of conductors is a Lyapunov function, and so the resistance is strictly decreasing. Several assumptions are required for the principle to be valid. The first of these is the assumption that the charge degrees of freedom relax on a timescale that is much faster than the mechanical degrees of freedom, and so can be neglected. This means the continuity equation for the charge density ρ may be simplified to

$$\frac{\partial \rho}{\partial t} + \nabla \cdot \vec{J} = \rho_s \rightarrow \nabla \cdot \vec{J} = \rho_s \tag{3.3}$$

Where ρ_s is a source term by which charge may be injected into the system. Secondly, the assumption is made that there are no notable sources of charge and so this can be simplified further as $\rho_s = 0$

$$\nabla \cdot \vec{J} = 0 \tag{3.4}$$

Under these two assumptions, the monopole charges on the conductors vanish and the interaction is due to image charge effects only. The dielectric medium is assumed to obey Ohm's law with conductivity σ, and so the electric field $\vec{E}$ between the conductors obeys the relationship

$$\vec{J} = \sigma \vec{E} \tag{3.5}$$

The electrical force $\vec{F}$ on the i^{th} conductor can be then written in terms of an integral over the surface S_i of the square magnitude of the electric field

$$\vec{F_i} = \frac{1}{2\epsilon} \int_{S_i} E^2 \hat{n}_i da_i \tag{3.6}$$

Where ϵ is the permittivity of the dielectric medium, $\hat{n}_i$ is the surface normal vector corresponding to the area element da_i. In the case of the 2D spherical conductors, the expression for the electric potential Φ is known in terms of the image charges to be

$$\Phi = \frac{Q_{ij}}{2\pi\epsilon} \ln\left(\frac{d_i}{d_j}\right) \tag{3.7}$$

Where Q_{ij} is the magnitude of the charges on each conductor and d_k is the distance to the k^{th} conductor. Using this, it is possible to calculate the electric field, and therefore the force between the conductors. This works out to give

$$\vec{F}_{ij} = -\frac{Q_{ij}}{4\pi\epsilon R} D_{ij} \tag{3.8}$$

For the two conductors separated by distance D_{ij}. Using the above assumptions and the electric potential of Eq. 3.7, an expression for the resistance between the two conductors can be found to be

$$R_{ij} = \frac{1}{\pi\sigma} \cosh^{-1}\left(\frac{D_{ij}}{2R}\right) \tag{3.9}$$

Taking the gradient of this and comparing to the form of the force $\vec{F}_{ij}$ gives a relationship between the gradient of the resistance and the force on the conductor

$$\vec{F}_{ij} = -\frac{\sigma}{2\epsilon} Q_{ij}^2 \nabla R_{ij} \tag{3.10}$$

Taking now the over damped approximation, the position $\vec{r}_i$ of the i^{th} conductor obeys the equation of motion

$$\dot{r}_i = -\frac{\sigma}{2\gamma\epsilon M} Q_{ij}^2 \nabla R_{ij} \tag{3.11}$$

For conductors of mass M and a damping coefficient of γ. The dynamics then always act to decrease the resistances given by R_{ij}.

3.2.2 Maximum entropy structures

An interesting experimental result suggests that a system of carbon nanotubes suspended in a non-conducting, non-polar fluid self organizes in such a way that the entropy production is maximized [2] in the presence of an applied voltage. When an electric field is applied between two parallel plate electrodes, nanotube structures grow, and an electrical connection between the plates is made. In the experiment, a resistor is connected in series with the electrodes. The resistance of the nanotube structures evolves over time, and tends towards equalling the value of the series resistance. This configuration is unique in that the power dissipation of the total system is maximized when the structure resistance reaches this value. This effect is observed to occur over a wide range of parameters. Figure 3.1 shows this behaviour for four values of the series resistor spanning several orders of magnitude.

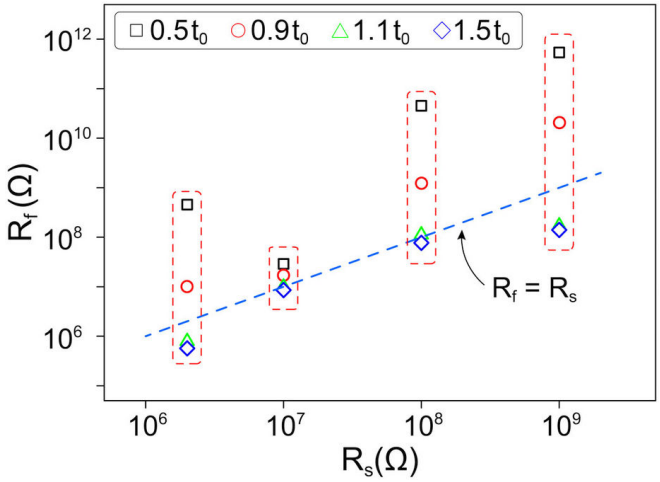

Figure 3.1: Evolution of self-organized nanotube structure resistance (R_f) over time. Blue diagonal line shows the value at which power dissipation is maximized for each value of the series resistance (R_s). Figure taken from [2].

This result is implies that the Maximum Entropy Production Principle of section 2.4.1 may be obeyed by this type of system for many parameter values. However, the guiding principles under which this behaviour occurs are still unclear, and the authors note that there is both a critical voltage below which the self-organization process does not yield complete connections, and a second critical voltage above which the self-organization is destroyed by

excessive heating and fluid flow.

3.2.3 Topological properties

A second interesting experimental result concerns the topology of electrical networks formed by a self-organization process. Several experiments[1, 3] have established the topology of 2D self-organized electrical networks is quite robust and repeatable. These networks are formed from metallic particles in a thin layer of viscous, insulating fluid when subject to a constant supply of electrical current.

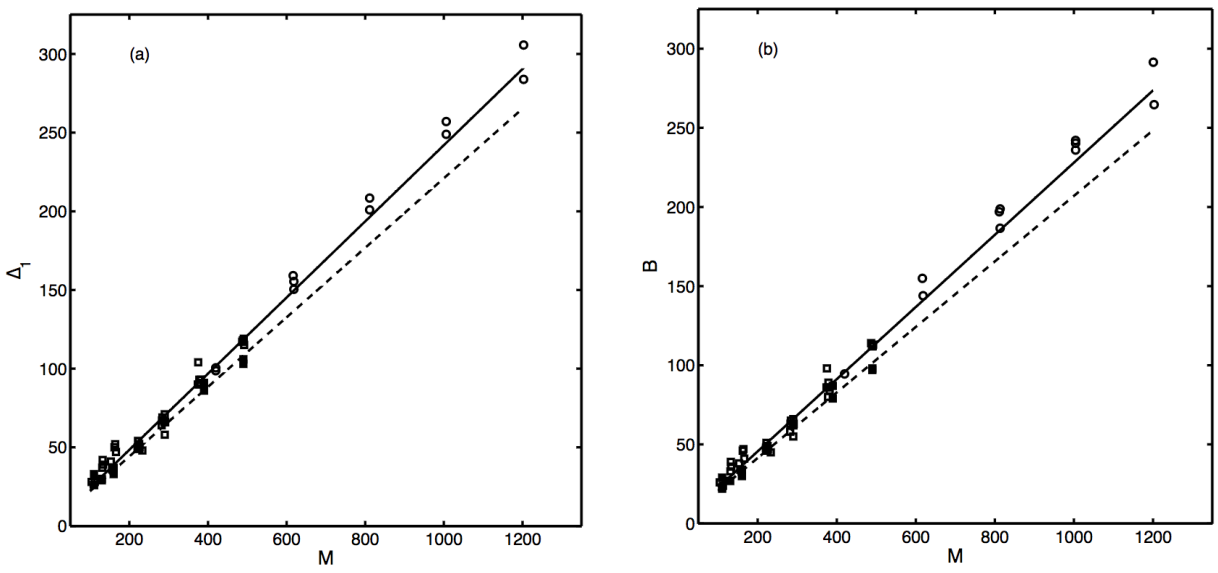

Figure 3.2: Measured number of network endpoints (Left) and branch nodes (Right). Circles represent experimental results from the self-organized particle network, while squares represent results from DLA simulations. Figure adapted from [3].

The left side of Fig. 3.2 shows one such result concerning the number of particles which have exactly one neighbouring particle (and are therefore endpoints). The right side shows a similar result for particles which have more than two neighbours (and are therefore branch points). In both cases, it can be seen that the fraction of nodes of each type is the same constant regardless of the size of the network. This result also demonstrates an interesting similarity in these values to those obtained from a diffusion limited aggregation (DLA) process, though it is at present unknown why this is the case. However, the similarity is not total[27], as DLA clusters differ slightly in other topological measures. As pointed out in [3], there is also similarity in the network topology to hydrological drainage networks (river networks) in the distribution of branches at various depths in the network. These results will be revisited again in Chapter 7, as one of the central goals of this work is to produce a physically accurate model which is capable of reproducing the correct network topology.

Chapter 4

Experimental results

4.1 Description of experiments

To determine the nature of the interaction forces that guide the self-organization process, two experiments were designed to directly probe an idealized self-organized wire[6]. Both experiments were carried out with a constant number of particles between two electrodes held at a fixed potential.

The first of these two experiments was aimed at identifying the mechanism of conduction through the system. In this experiment, a single particle was placed in the gap between two electrodes and allowed to transport charge between them. The electrical current between the electrodes was measured as a function of the size of the gap g between the electrodes. A diagram of the experimental setup used to measure the charge carried by a single conductor can be seen in Fig. 4.2.

For this experiment the potential difference between the electrodes was held fixed at $18kV$, and the radius of the conducting particle was $R = 0.775mm$. The time-averaged current was measured by inserting a $10k\Omega$ resistor between one of the electrodes and the voltage source and measuring the voltage drop.

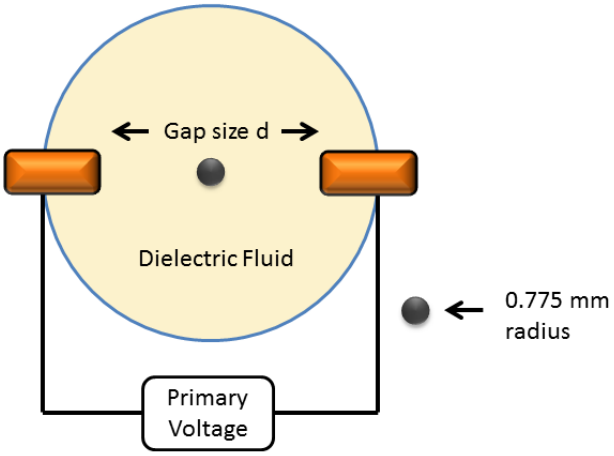

Figure 4.1: Diagram used to measure the charge carried by a single conductor

The second experiment was designed to probe the conductor-conductor interaction forces. To do this, the previous setup was modified to include $N = 25$ conductors which form an almost complete wire between the two primary electrodes. In addition, a pair of secondary electrodes were added which run parallel to the wire and create a transverse electric field. Screens were inserted between the wire and the transverse electrodes to prevent an accidental electrical discharge from the primary voltage source to the transverse voltage source.

The transverse electric field caused a distortion in the wire, and above a critical value caused the wire to become unstable. The distortion in the wire and the critical transverse field strength are both closely related to the electrostatic interactions between the conductors, and so this measurement provides a way to probe the importance of these interactions.

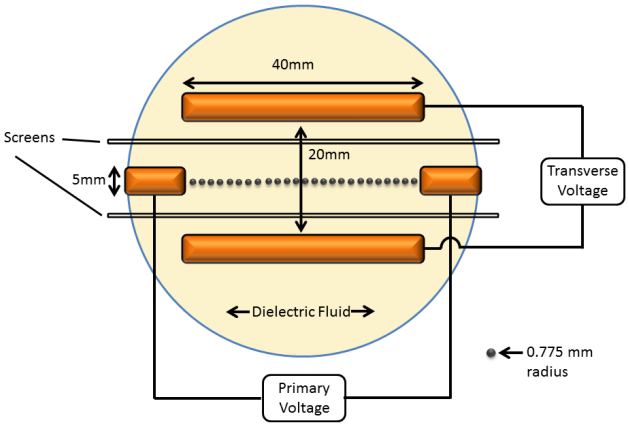

Figure 4.2: Diagram used to measure the conductor-conductor interaction forces and stability of the self-organized wire

The results of these experiments directly informed the modeling and analysis carried out in chapters 5, 6, and 7.

4.2 Conductivity theory and measurement

Since the conductor is free to move in the gap between the electrodes, it will become polarized and be drawn to either one of the electrodes. When contact occurs between the conductor and the electrode, the conductor will acquire a net charge Q of the same sign as the electrode it is in contact with, and be repelled back into the gap. The conductor's net charge then causes it to be attracted to the opposite electrode, and the process repeats. In this way, the single conductor acts as a charge shuttle moving electric charges across the gap between the electrodes[28] as it oscillates back and forth. On each trip across the gap, the conductor carries an amount of charge

$$Q = CV \tag{4.1}$$

Where C is the capacitance of the conductor and V is the potential of the electrode it was last in contact with. The time averaged current can then be related to the frequency $\gamma\phi$ of

the conductor oscillations by

$$I = Qf \tag{4.2}$$

The frequency of oscillations can be computed by taking the overdamped approximation to the motion of the particle. Assuming stokes drag of the form γv and taking the monopole approximation to the electric force, equation of motion of the conductor in the gap is

$$\dot{x} = \frac{2\left(C\Delta V\right)^2}{4\pi\epsilon\gamma}\frac{\left(g+4R\right)^2+4x^2}{\left(g+4R\right)^2-4x^2} \tag{4.3}$$

From this the frequency of oscillations can be computed as

$$f^{-1} = \frac{C}{A}\left[(g+4R)^3\arctan\left(\frac{g}{g+4R}\right) - \frac{2}{3}g(g+3R)(g+6R)\right] \tag{4.4}$$

where A is defined as $A = 2C^3(\Delta V)^2/(4\pi\epsilon\gamma)$. This gives the following equation for the conductivity σ of the gap with the charge shuttle:

$$\sigma = A\left[(g+4R)^3\arctan\left(\frac{g}{g+4R}\right) - \frac{2}{3}g(g+3R)(g+6R)\right]^{-1} \tag{4.5}$$

The electrical resistance R_E of the gap with the charge shuttle is then

$$R_E = \frac{1}{A}\left[(g+4R)^3\arctan\left(\frac{g}{g+4R}\right) - \frac{2}{3}g(g+3R)(g+6R)\right] \tag{4.6}$$

Figure 4.3 shows a plot of Eq. 4.6 with the best fit value of the parameter A as compared to experimental results for a variety of gap sizes. The experiment was carried out using the setup diagrammed in Fig. 4.2 with a conductor of radius $R = 0.775mm$ and a potential difference of $\Delta V = 18kV$.

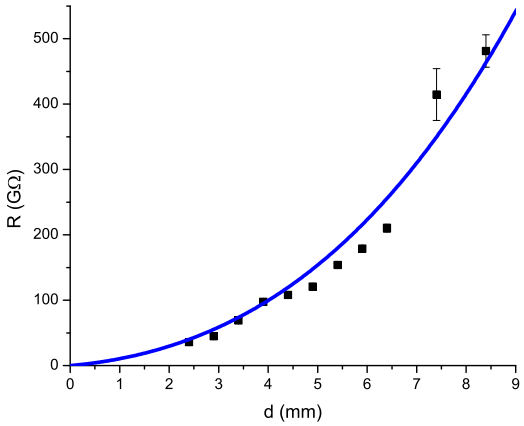

Figure 4.3: Electrical resistance of the gap containing a single conductor as a function of gap size g compared to the best fit (blue line) of Eq. 4.6

It can be seen from this experiment that the presence of the mobile conductor leads to an electrical resistance that is nonlinear in the size of the gap. Furthermore, Eq. 4.6 agrees very well with the experimentally measured results, and also predicts that the resistance is non-ohmic. By inspecting the quantity A it can be seen that the movement of the conductor in the gap causes the electrical resistance to decrease with increasing voltage. Specifically, a dependence of the form

$$R_E \sim \frac{1}{(\Delta V)^2} \tag{4.7}$$

arises due to the increasing oscillation frequency at higher voltages.

4.3 Stability theory and measurement

For the case of an almost complete idealized multi-conductor wire, it is possible to calculate the stability properties directly using a few simplifying assumptions. First, it is assumed that a straight wire has formed between two electrodes held at a fixed potential difference ΔV. This idealized wire is complete with the exception of agap of size g between two of its constituent conductors. Since there are N conductors in the wire, this gap may occur in

$N+1$ different locations. It is assumed that the gap is equally likely to occur at any one of the possible locations. The electric potential of the conductors on either side of the gap will be equal to the potential of the electrode that they are connected to by the rest of the complete wire. A simplified diagram of this situation can be seen in Fig. 4.4.

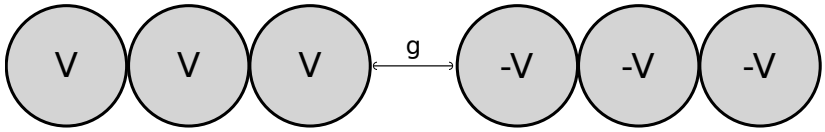

Figure 4.4: A gap of size g in an otherwise complete wire

Under the additional assumption that the number of conductors in the wire is long, the capacitance C of the conductors is identical regardless of their position along the wire. In this case, conductors on one side of the positive potential side of the wire (called the left side) experience a force of

$$\langle F_{i\in\text{left}}\rangle = C\Delta V E_{\perp} \tag{4.8}$$

Where i is the conductor index and $E_{\perp}$ is the component of the electric field perpendicular to the wire which is generated by the secondary electrodes. The conductors on the negative potential side (the right side) of the gap experience the opposite force

$$\langle F_{i\in\text{right}}\rangle = -C\Delta V E_{\perp} \tag{4.9}$$

The average force on the i^{th} conductor can be found by averaging over all the $N+1$ positions of the gap. Letting the conductor index $i \in \{1, 2, ..., N\}$ run from left to right implies that there is an $\frac{i}{N+1}$ probability of the i^{th} conductor being on the right side of the gap, and a $\frac{N+1-i}{N+1}$ probability of the i^{th} conductor being to the left of the gap. Thus the average force on the i^{th} conductor is given by

$$\langle F_i\rangle = -\frac{C\Delta V E_{\perp}}{2(N+1)}\,(N+1-2i) \tag{4.10}$$

This force is perpendicular to the wire and decreases linearly along its length. For small values of $\langle F_i \rangle$, a small distortion of the previously straight wire results. Figure 4.5 shows a photo of the unperturbed and perturbed wire which has been disorted by the transverse electric field.

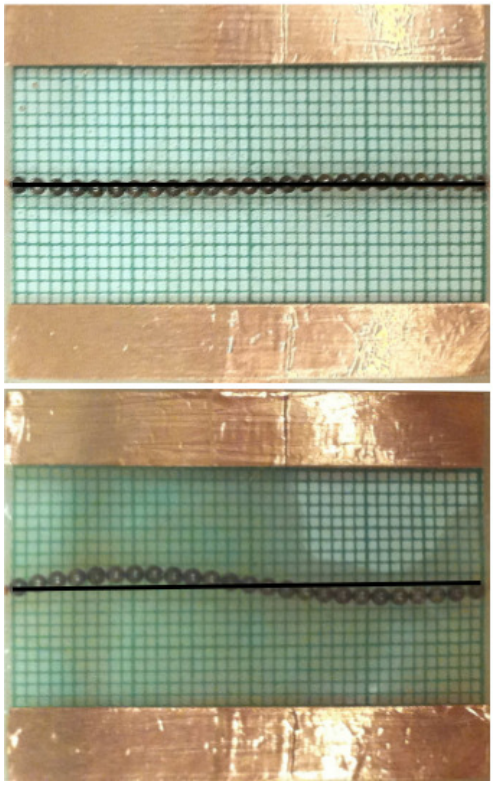

Figure 4.5: Top: unperturbed wire. Bottom: Wire pertubed by a $2kV$ voltage on the transverse electrode.

Provided the displacement is small, the total length of the wire is not significantly different from its unperturbed length L, and the size of the gap may be approximated as

$$g \approx \frac{L - 2NR}{N + 1} \tag{4.11}$$

The stabilizing force which is parallel to the wire can be evaluated using the force F_2between

two conducting spheres in close approach[29]

$$F_2 = \frac{1}{4\pi\epsilon}\frac{Q^2}{2Rg\left(\ln\left(\frac{4R}{g}\right)+2\gamma_e\right)^2} \tag{4.12}$$

where γ_e is the Euler-Mascheroni constant. With this, the stabilizing force T which acts parallel to the wire is

$$T = \frac{1}{4\pi\epsilon}\frac{C^2(\Delta V)^2(N+1)}{2R(L-2NR)\left(\ln\left(\frac{4R(N+1)}{(L-2NR)}\right)+2\gamma_e\right)^2} \tag{4.13}$$

This force plays the role of an effective tension in the wire, and acts to stabilize it against external perturbations.

4.3.1 Wire distortion curve

With the effective tension force along with the perpendicular force, the displacement of the wire in the perpendicular electric field can be calculated. It is convenient to do this in the limit of a long wire, which entails taking the continuum limit. This is the limit in which $i \to x(N+1)/L$ and $\langle F_i\rangle \to \langle F(x)\rangle = -C\Delta V E_\perp(1/2 - x/L)$. The motion of the wire is subject to a viscous damping of the same form of the damping on an individual conductor. This idealized wire is then governed by the following equation of motion:

$$\rho\ddot{y}(x) = Ty''(x) + \langle F(x)\rangle\, L - \gamma\dot{y}(x) \tag{4.14}$$

With boundary conditions such that $y(0,t) = 0$ and $y(L,t) = 0$. In the steady state, $\ddot{y}(x) = \dot{y}(x) = 0$ and the stationary configuration of the wire can be evaluated. The steady state displacement of the wire is then

$$y(x) = B\left(x - \frac{L}{2}\right)(L-x)\,x \tag{4.15}$$

Where the quantity B is defined as $B = \frac{6C\Delta V E_\perp}{L^2 T}$.

Figure 4.6 shows a comparison between the curve defined by Eq. 4.15 and the experimentally measured wire distortion. The experiment was carried out with $N = 25$ conductors in the wire, a primary electrode potential difference of $\Delta V = 18kV$ and a secondary electrode voltage of $\Delta V_\perp = 2kV$. The total distance between the primary electrodes was $L = 40mm$. As in the conductivity measurement, conductors of radius $R = 0.775mm$ were used. The best fit value for the quantity B was used for the comparison. The measured wire displacements were averaged over five different experiments.

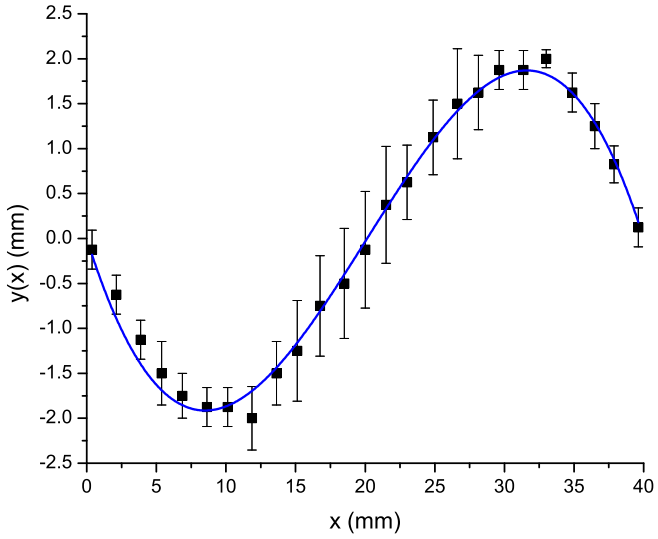

Figure 4.6: Comparision between the experimentally measured wire distortion and the best fit form given by Eq. 4.15

4.3.2 Maximum displacement

In addition to calculating the shape of the distorted wire, the maximum displacement y_{max} can also be calculated from Eq. 4.15. This is

$$y_{max} = \frac{6\Delta V L}{12\sqrt{3}} \frac{C}{T} E_\perp \tag{4.16}$$

This implies that the amplitude of the wire displacement grows linearly with the perpendicular field. Figure 4.7 shows the experimentally measured maximum distortion of the wire as a function of applied transverse voltage. The experiments were carried out using the same setup as in section 4.3.1,

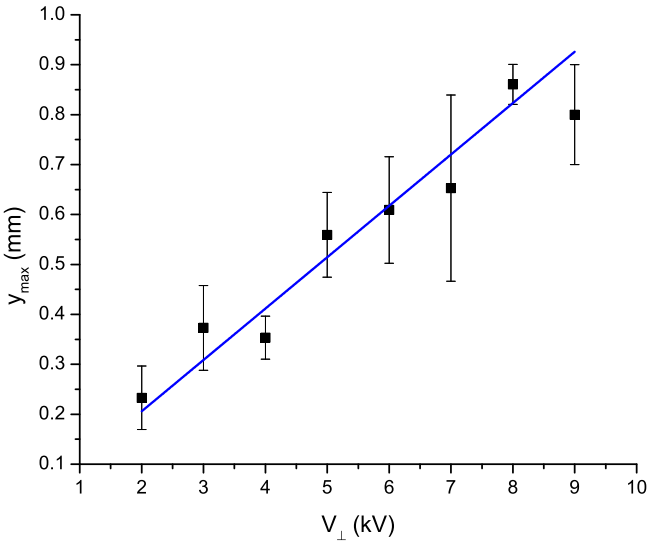

Figure 4.7: Comparision between the experimentally measured wire distortion and the best fit form given by Eq. 4.15

While noisy, it can be seen that the maximum distortion of the wire increases linearly with the applied transverse voltage in accordance with Eq. 4.16.

4.3.3 Critical transverse voltage

The distortion characterized in Eq. 4.15 and Eq. 4.16 only occurs for transverse voltages below a critical voltage V_C. Above this voltage, the wire loses stability and breaks apart. This occurs when the wire distortion is large enough that the effective tension of Eq. 4.13 is no longer perpendicular to the force caused by the transverse voltage given by Eq. 4.10. The component of the tension force which is parallel to (and thus counter-acted by), the

force due to the transverse field is given by

$$T = \langle F_i \rangle \sin\theta \tag{4.17}$$

The minimum transverse voltage at which the wire can break is therefore governed by the maximum transverse force, $F_{max} = \frac{\mathcal{C}\Delta V E_\perp}{2}$, and the maximum value of $\sin\theta$. The $\sin\theta$ term can be computed from the relationship

$$\sin\theta = \frac{\frac{dy}{dx}}{\sqrt{1+\frac{dy}{dx}}} \tag{4.18}$$

with y from Eq. 4.15. The maximum value is obtained when

$$\frac{dy}{dx} = 24\frac{F_{max}}{T} \tag{4.19}$$

This gives the relationship between the wire tension and the transverse field at which breakage may occur as

$$E_\perp = \sqrt{2+\frac{\sqrt{145}}{6}}\left(\frac{T}{\mathcal{C}\Delta V}\right) \approx 2.002\left(\frac{T}{\mathcal{C}\Delta V}\right) \tag{4.20}$$

Under the approximation $\mathcal{C} \approx 4\pi\epsilon R$, and with the largest possible gap size, this can be written as

$$E \approx 2.002\frac{E_\parallel L}{2(L-2NR)(N+1)\left(\ln\frac{4R(N+1)}{L-2NR}+2\gamma\right)^2} \tag{4.21}$$

Using the experimental parameter values, and the above approximations, the theoretically calculated critical field from Eq. 4.21 is $E_\perp \approx 334\frac{kN}{C}$ which corresponds to a critical transverse voltage of $V_C \approx 6.7kV$. The experimentally measured result is $V_C = 8.5 +/- 0.7kV$, which is likely due to the capacitance being overestimated in the isolated sphere approximation.

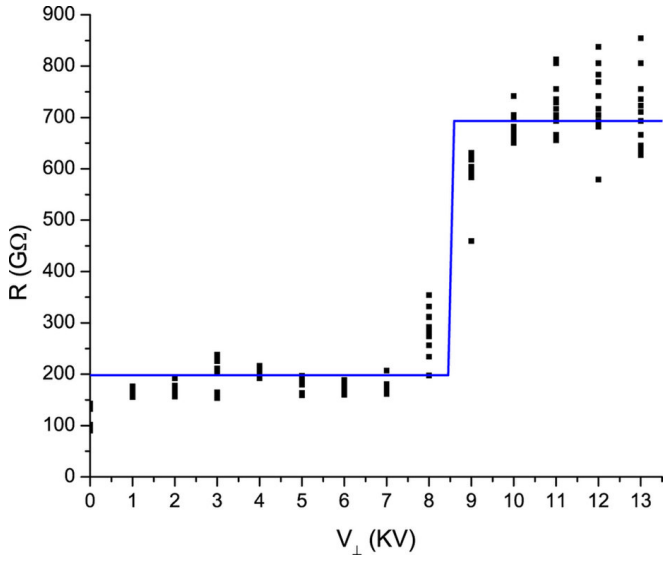

Figure 4.8: Resistance as a function of transverse voltage showing the resistance increase as the wire breaks. The blue line is a best fit step-function with a low resistance of $R = 198G\Omega$ and a high resistance of $R = 693G\Omega$ with the transition at $V_C = 8.7kV$.

The wire breaking transition can be clearly seen in a plot of wire resistance as a function of transverse voltage, as in Fig. 4.8. The transition occurs over a fairly narrow voltage range, and is associated with a resistance increase of over a factor of two.

4.4 Interpretation and implications

The above experimental results and theoretical work indicate two important properties of these self-organizing particle structures that must be carefully accounted for in any complete model of the system. First, the surface charge on each conducting object is relevant for both the conductivity of the system as (Section 4.2) and the stability of the stationary state (Section 4.3). This is contrary to the assumptions used to derive the minimum resistance principle[5] (Section 3.2.1), in which the conductors were assumed to discharge rapidly into the surrounding environment. Second, the higher order multipole interactions are responsible for the attractive forces which cause the conductors to combine into more complex structures. It is the interplay between the attractive higher order interactions and

the monopole interactions that drive the self-organization. It is necessary to model both of these effects accurately if the model is to faithfully reproduce the behavior of the real system.

Chapter 5

Theoretical modeling

5.1 Necessary components

To accurately model the self-organization process, there are several necessary components which derive both from general thermodynamic considerations as well as system specific properties. At a high level, owing to general properties of nonequilibrium structure formation [19, 30], the model must contain both a coupling to an energy source as well as a mechanism by which energy can be dissipated. In the following model, the dissipation mechanism will take the form of a viscous drag (Stokes drag) due to the motion of the conductors through the fluid medium. The theoretical treatment due to Dueweke[5] highlights the convenience gained by taking the drag force to be large, such that the motion is nearly overdamped. This is in line with much of the experimental work [6, 3, 1], which considers systems in very thick fluids, such as Castor oil. In the following model, a viscous fluid will be assumed, which will aid in the convergence of numerical calculations, but in contrast to the previous theoretical treatments, the overdamped approximation will not be used.

While the dissipation mechanism is relatively simple, the source of energy for this system is somewhat more complex. Electrical energy will be supplied to the system via two different mechanisms. First, and perhaps the most straightforward, an electrostatic boundary condition will be imposed by the presence of a ground electrode. This electrode will serve as a reference potential (its surface potential will be held at a fixed zero value) regardless of the configuration of the rest of the system. This induces image charges on the surface of the free conductors in the system, and so raises the internal energy. Second, energy will directly

be supplied in the form of a constant direct current flowing into each of the conductors in the system. In experimental systems, this current is supplied via field emission from a sharp metal needle above the system which is held at a high voltage[3, 1]. It is the interplay between this energy source and the dissipation that is at the heart of the self-organization process.

In addition to these two general features of the system, there are a few properties specific to the conductor system under consideration that must be modeled. The most difficult of these is the accurate modeling of the electronic interaction between the different conductors, which requires accounting for the image charge effects due to every charged surface in the system. In addition to this, special care will be given to the calculation of both the mechanical degrees of freedom as well as the electrical degrees of freedom during a collision between two conductors. Consideration must also be given towards assigning physical values to the free parameters of the model.

In the following, the various important approximations will be discussed, and the electrical degrees of freedom will be modeled. Then, the model of mechanical degrees of freedom will be developed and the dynamics during conductor contacts will be specified. After this, the free parameters of the model will be assigned values such that comparison to physical systems is possible. The result is a model that has the features discussed above and can be treated numerically.

5.2 Approximations

5.2.1 Electrostatic approximation

This model considers the case of N spherical conducting objects of radius R. Unless otherwise indicated, the conductors will be enumerated using the index $i \in \{1, 2, ..., N\}$. In general,

the electric potential in the region between the conductors obeys Maxwell's equations

$$\begin{gathered}\nabla^2 V(\vec{r},t) - \frac{\partial}{\partial t}\left(\nabla\cdot\vec{A}\right) = -\frac{\rho}{\epsilon} \\ \left(\nabla^2 A - \frac{1}{c^2}\frac{\partial^2 A}{\partial t^2}\right) - \nabla\left(\nabla\cdot A + \frac{1}{c^2}\frac{\partial^2 V(r,t)}{\partial t^2}\right) = -\mu\vec{\mathcal{J}}\end{gathered} \tag{5.1}$$

Where $V(\vec{r},t)$ is the electrostatic potential, $\vec{A}$ is the electromagnetic vector potential, ϵ is the permittivity of the medium, and ρ is the charge density in the medium. However, experimental results, such as the resistivity and charge transportation measurements in Chapter 4 suggest that in actuality, the electrical currents through the system are very small (on the order of $10^{-9}A$), while the electrostatic forces are responsible for the mechanical motion of the conductors. This implies that the magnetic effects in Eq. 5.1 can safely be ignored. This entails making the approximation

$$\frac{\partial^2 V(r),t}{\partial r^2} \gg \frac{1}{c^2}\frac{\partial V(\vec{r,t})}{\partial t^2} \tag{5.2}$$

Along with $\vec{A} \approx 0$. In addition, the medium is assumed to be a perfect electrically neutral insulator. After this, the electric potential in the region between conductors is described by the Laplace equation

$$\nabla^2 V(r,t) = 0 \tag{5.3}$$

This is the most important approximation in the model developed in this chapter, as it renders the problem numerically tractable.

5.2.2 Ideal conductor approximation

In addition to and supporting the electrostatic approximation, the conductors will also be assumed to act as perfect conductors in that charge added to their surface instantaneously relaxes to its equilibrium distribution. The importance of this assumption is that under this condition, all points on the surface of a conductor will have the same electric potential. This

is particularly useful in specifying the boundary conditions of Eq. 5.3. This in turn aides the calculation of the conductor-conductor interaction forces which arise from image charge effects, as the surface charge distribution is simply related to the solution of Eq. 5.3. As part of this assumption, the conductors are also assumed to not have any internal magnetic dipole moments.

5.2.3 Collision approximations

During the time evolution of the system, it will be necessary to treat the case in which two or more conductors collide. The treatment of collision dynamics between rigid objects is known to be quite difficult[31], and so special care must be taken to treat the contact mechanics accurately. The model developed in this chapter will make use of the assumption that the collisions are elastic. An additional assumption that will be used is that the collisions are frictionless, meaning that the contact forces have no components parallel to any surfaces involved in the interaction. These two assumptions restrict the possible contact interactions that may be used, although many physically interesting interactions (eg. Van der Waals type interactions) are still possible. Although a specific choice of interaction is used in this work, in principle any interaction with the above properties may be used. A final assumption that is both physically motivated and useful for calculations is that the conductors are not deformed during a collision.

5.3 Electrical degrees of freedom

The primary interaction between conductors in the system is electronic in nature, as it is the buildup of excess charge on the conducting surfaces that drives the motion of the system. Therefore, the modeling of the electronic degrees of freedom specifies much of the system behavior. The three electronic degrees of freedom present in this model are the electric potential $V(\vec{r}.t)$, the electric charge of each conductor Q_i, and the electric force on

a conductor $\vec{F}_i(t)$ for $i \in \{1, 2, ..., N\}$.

The behavior of the first of these, $V(\vec{r}.t)$ is essentially captured in the partial differential equation of Eq. 5.3. However, the solution of this requires appropriate boundary conditions. One such boundary condition is given by the assertion that the ground electrode is held at a fixed zero reference potential, which specifies a Dirichlet boundary condition on the solution. The remaining boundary conditions are generated from the total charge Q_i on each conducting surface. These values are related to the electric potential by the surface integral

$$Q_i = -\epsilon \int_{\partial\Omega_i} \frac{\partial V(\vec{r}, t)}{\partial n_i} \tag{5.4}$$

Where the integral over $\partial\Omega_i$ corresponds to the integral over the surface of the i^{th} conductor, and n_i is a unit vector normal to the surface. In principle, if all the conductor charges are known, the solution to Eq. 5.3 is well defined. However, the actual calculation of the solution with these boundary conditions is somewhat involved. Methods for dealing with these types of boundary conditions are developed in section 6.5.

The conductor charges themselves change in time, due to both the supplied current as well as the flow of charge between conductors in contact. In the absence of conductor-conductor contacts, the time evolution of the charges follows the equation

$$\dot{Q}_i(t) = J \tag{5.5}$$

Here J is the current flowing into the conductor from the current supply. The charge on the conductor increases monotonically until the electrical forces are great enough that the conductor moves into a position where it can discharge, either to another conductor or to the ground electrode.

The forces arising from the conductor charges can be calculated from the solution of Eq.

5.3 via another surface integral similar to the calculation of the conductor charges.

$$\vec{F}_i(t) = \frac{\epsilon}{2} \int_{\partial\Omega_i} \left(\frac{\partial V(\vec{r}, t)}{\partial n_i} \right)^2 \hat{n}_i \tag{5.6}$$

As before, the integral is taken over the surface of the conductor, however the direction of the force at each infinitesimal is specified by the surface normal.

Together, the equations 5.4, 5.5, and 5.6 specify the electronic degrees of freedom of the model. These quantities are related to the electric potential, and therefore to the solution of Eq. 5.3. In principle these degrees of freedom can be calculated given a known initial condition consisting of the positions (and geometry) of each conductor and the total charge on each conductor. Methods of doing this calculation numerically will be developed in chapter 6.

5.4 Mechanical degrees of freedom

While the main forces that guide the self-organization process of the system are electrical, it is also necessary to specify the mechanical degrees of freedom to fully describe the system behavior. In order to solve the initial value problem, these are best expressed as first order differential equations. For each conductor, there is then a set of $2D$ mechanical degrees of freedom in D dimensions. These are

$$\begin{aligned} \dot{\vec{r}}_i &= \frac{\vec{p}_i}{m_i} \\ \dot{\vec{p}}_i &= \vec{F}_i(t) - F_{drag}\left(\vec{p}_i\right) + \sum_{j=0}^{N} F_{contact}\left(\vec{r}_i - \vec{r}_j\right) \end{aligned} \tag{5.7}$$

Where $\vec{r}_i$ is the position of the i^{th} conductor, $\vec{p}_i$ is the momentum, both of which are time dependent quantities, and m_i is the mass.

5.4.1 Fluid drag

To complete the description, two additional interactions, the drag force and the contact force must be specified. For the rest of this work, the simplest physically reasonable choice of the drag force will be assumed, which is Stokes drag

$$F_{drag}\left(\vec{p}_i\right) = \frac{\gamma_i}{m_i}\vec{p}_i \tag{5.8}$$

Here the drag coefficient γ_i can be expressed in terms of the dynamic viscosity η of the medium via $\gamma_i = 6\pi\eta R$ for spherical objects [32]. This choice greatly simplifies the model as it abstracts away nearly all of the complex fluid interactions. This is the mechanism by which excess mechanical energy in the system is dissipated. Other choices of drag force, including choices informed by more detailed fluid dynamics are possible, but are not necessary for the self-organization to occur.

5.4.2 Contact dynamics

In addition to the choice of fluid drag, the conductor-conductor interaction force must also be chosen. Here, due to the simplifying assumptions made in section 5.2, classical contact theory for non-adhesive elastic contact may be applied. For this type of contact, the interaction force between two spherical conductors [33] is

$$F_{contact}\left(\vec{r}_i - \vec{r}_j\right) \propto \begin{cases} R^{1/2}\left|r_i - r_j\right|^{3/2} & \text{for } |r_i - r_j| < R \\ 0 & \text{otherwise} \end{cases} \tag{5.9}$$

This choice includes the elastic effects due to the deformation of the materials in contact, up to a proportionality constant κ. For stiff materials, such as steel, this proportionality constant is typically quite large, and the deformation as measured by $|r_i - r_j|$ is correspondingly small.

As with the fluid drag, there are many possible choices for the form of the contact interaction force, and the one chosen here is in some sense the minimal choice in accordance with the simplifying assumptions of section 5.2. More detailed information about the surface interactions between the conductors may be included here.

5.5 Complete model

For completeness, and later reference, the full set of model equations is restated here:

$$\begin{aligned}
&\nabla^2 V(r,t) = 0 \\
&Q_i = -\epsilon \int_{\partial\Omega_i} \frac{\partial V(\vec{r},t)}{\partial n_i} \\
&\dot{Q}_i(t) = J \\
&\vec{F}_i(t) = \frac{\epsilon}{2} \int_{\partial\Omega_i} \left(\frac{\partial V(\vec{r},t)}{\partial n_i} \right)^2 \hat{n}_i \\
&\dot{\vec{r}}_i = \frac{\vec{p}_i}{m_i} \\
&\dot{\vec{p}}_i = \vec{F}_i(t) - F_{drag}\left(\vec{p}_i\right) + \sum_{j=0}^{N} F_{contact}\left(\vec{r}_i - \vec{r}_j\right)
\end{aligned} \tag{5.10}$$

A solution of these six equations from appropriate initial conditions and parameter values gives the output of the model.

5.5.1 Initial conditions

For simplicity, the initial velocities of all conductors will be assumed to be zero, $p_i(0) = 0$ $\forall i \in \{1, 2, ..., N\}$. The initial conditions for the mechanical degrees of freedom are therefore a set of initial conductor positions $\{\vec{r}_1, \vec{r}_2, ..., \vec{r}_N\}$. The electric charges of each conductor will be initialized to zero $Q_i(0) = 0$ $\forall i \in \{1, 2, ..., N\}$. Similarly, the initial value for the electric potential is also initialized to zero $V(r, 0) = 0$ $\forall \vec{r}$. This implies the surface potentials of all conductors is likewise zero $V_i(0) = 0$ $\forall i \in \{1, 2, ..., N\}$, and so this quantity need not

be calculated initially. At time $t = 0$, the ground electrode potential will be set to $V_0 = V_g$, after which this quantity will be held fixed. This represents the switching on of the external voltage source as in experiments. These initial conditions are not the only choices, but will be the ones used for the numerical experiments in this work.

5.5.2 Free parameters

To evaluate the model, it is also necessary to specify the value of the various physical parameters. While the behavior of the model does not have any obvious sensitive dependence on the physical parameters, these are ideally chosen to allow comparasions to the existing experimental data. In total, there are three electrical parameters of importan ce, and a set of $2 + N$ unique mechanical parameters that relate to the properties of the materials the conductors are made of as well as the fluid medium.

Of primary importance is the ground electrode potential V_g, which for this work was set to $V_g = 0$. This choice is in fact somewhat irrelevant as the system dynamics ultimately only depend on differences in potential. Therefore, this choice, along with the initial conditions from Section 5.5.1 implies that there are initially no transient electronic forces, and the electrical forces are slowly activated as charge on the conductors increases due to the current source. This quantity was given a value in accordance with the power supply voltage and measured resistance from Chapter 4. Assuming a power supply voltage of $\sim 20kV$ and an open circuit resistivity of $\sim 200G\frac{\Omega}{cm}$, and a $\sim 5cm$ experiment, the applied current can be set to $J = 0.2nA$. For the final electrical parameter, the value of the permittivity of the medium was chosen to be $\epsilon = 4.7\epsilon_0$, which is the well known measured value for castor oil [34].

The remaining parameters that must be specified are mechanical. As the permittivity of the insulating medium was set to be the value for castor oil, the fluid viscosity is likewise set to the viscosity of castor oil. This amounts to chosing the dynamic viscosity $\eta = 700cP$ for castor oil[35] at $22°C$. As for the fluid medium, the conductor properties will be specified

by first making the selection that the conductors are made of steel, as in the experiments of Chapter 4. This specifies the mass of each of the conductors to be $m_i = \frac{4}{3}\pi\rho_{steel}R_i^3$ with $\rho_{steel} = 8050kg/m^3$ as the mass density of steel[36]. Likewise, the stiffness of the material should be chosen to be the appropriate value for steel, which has a Young's modulus of $Y \approx 200GPa$[37]. This value allows the calculation of the contact force, although in practice any sufficiently large value will have a similar effect. These values complete the model, and will be the values used in the rest of this work. In principle, as the model is now fully specified, calculations may be performed. However, a great deal of care must be taken to ensure that the result remains physical. Chapter 6 will be devoted to doing calculations with this model.

Chapter 6

Numerical Methods

6.1 Introduction

The model described in section 5.5 is complete in the sense that is can be used to calculate the state of the system at any time. However, such calculations are exceedingly difficult to do analytically. It will be the goal of this chapter to develop a numerical means of exploring the behavior of this model. To do this will require moving to discrete time and propagating an initial state of the system forward for the desired amount of time.

Propagating a state forward for one time step requires several parts. From the previous state, the electric potential must be computed, which in turn requires a computation of the potential boundary conditions. From this, the force on each object must be calculated, which then allows the numerical integration of the equations of motion. These steps must be iterated on every time step, and the number of iterations will determine the overall numerical accuracy achieved. A flow chart showing the relationship between these steps can be seen in Figure 6.1.

As the amount of computation required for each time step is significant, and a large number of time steps will be required, special care will be taken to develop an efficient and scalable numerical procedure. Since the model in section 5.5 has been formulated in terms of the electric potential, a great deal of speed can be gained by using a parallel method for the computation of this quantity.

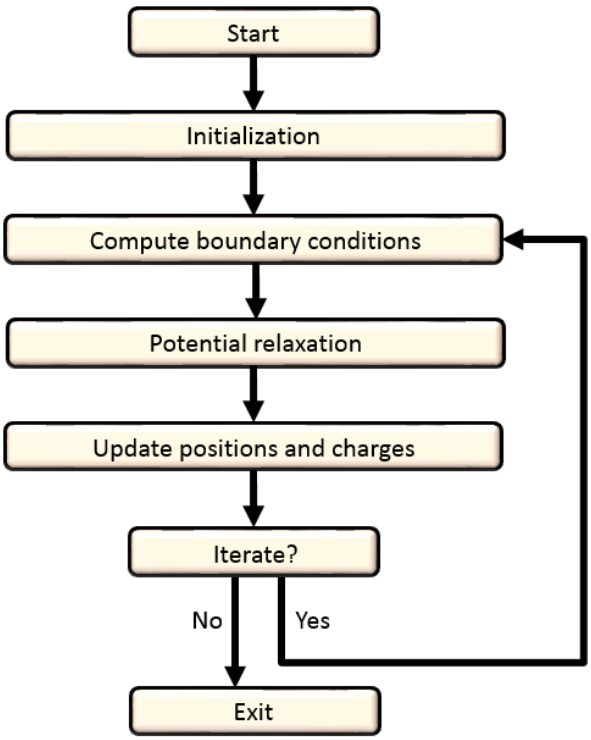

Figure 6.1: Flow chart of the algorithm

6.2 Compute Unified Device Architecture (CUDA)

The framework used for the implementation of this algorithm was the Compute Unified Device Architecture (CUDA) developed by Nvidia for general purpose computing on graphics processing units (GPUs)[38]. This architecture allows massively parallel algorithms to be developed which run on Nvidia GPUs. All computations were run on a combination of a Nvidia Tesla C2050 GPU Computing Module and a Nvidia GeForce GTX 550 Ti. Use of the massively parallel GPU computing modules drastically reduces the computation time required to solve for the electric potential.

6.3 Solution for the electric potential

In order to numerically evaluate the model outlined in section 5.5, it is imperative that solutions to the equation

$$\nabla^2 V(x, y, t) = 0 \tag{6.1}$$

in the 2D region of interest can be generated quickly and with minimal overhead. This is because a new solution for the electric potential is required every time the conducting particles move. Many numerical methods exist to solve this type of problem[39], however, due to the computing model discussed in section 6.2, only a select few make good candidates. The requirements are such that the solution algorithm must have the following properties:

1. Compatibility with all boundary conditions
2. Fully explicit
3. Numeric stability
4. Relatively quick convergence without excessive memory overhead

One algorithm that is straightforward to implement and satisfies all of these requirements is the Gauss-Seidel algorithm with red-black ordering [39, 40, 41, 42, 43]. This is a finite-difference method, and as such requires a discretization of the region of interest.

Once the discretized solution is obtained, interpolation[44, 45] can be used to up-sample the solution and allow for an approximation of the electric potential to be obtained for all locations in the region of interest.

6.3.1 Discretization scheme

The 2D region of interest is taken to be a square region. In previous work, the side length of this region was $L = 5.12cm$ in physical units. Calling $S = 512$ the number of sites in

each direction, the discretization yields a square lattice of $S \times S$ sites with a separation of $0.1mm$. The discretized electric potential is then written as

$$V(x, y, t) \approx V_{i,j}(t) \tag{6.2}$$

where $i, j \in \{0, 1, 2, ..., S-1\}$. The convention used for rendering images has the point $(i, j) = (0, 0)$ as the bottom left corner of the image.

6.3.2 Boundary conditions

The discretized boundary conditions are relatively straightforward. A point (i, j) on the discrete lattice corresponds to a point (x, y) in the physical region of interest given by the equations

$$\begin{aligned} x &= \frac{i}{S}L \\ y &= \frac{j}{S}L \end{aligned} \tag{6.3}$$

If the point (x, y) lies within the surface of a conducting particle, then the point (i, j) is held at a fixed potential equal to the potential of that conduction particle. This corresponds to imposing a Dirichlet boundary condition on the surface of each conductor.

In addition to these boundary conditions, it is also necessary to specify how the electric potential behaves on the edges of the region of interest. A logical choice are open or Von-Neumann boundary conditions, in which the first derivative of the electric potential is constrained to be zero on the edges of the region of interest. This can be accomplished by assigning values to the discretized electric potential on lattice sites that are immediately

outside the region of interest:

$$\begin{aligned} V_{-1,j} &= V_{0,j} \\ V_{i,-1} &= V_{i,0} \\ V_{S,j} &= V_{S-1,j} \\ V_{i,S} &= V_{i,S-1} \end{aligned} \tag{6.4}$$

With these boundary conditions, the solution for the electric potential is uniquely defined for any given set of conductor surface potentials.

6.3.3 Electric potential relaxation

With this discretization, the Red-Black Gauss-Seidel algorithm provides simple update rules for the electric potential $V_{i,j}(t)$. First, each site is assigned a label, either Red or Black. This assignment must be done so that the label of each site is different from the label of every adjacent site. The simplest way of assigning these labels is as follows:

$$\text{label} = \begin{cases} \text{Red} & \text{if } (i \bmod 2) = (j \bmod 2) \\ \text{Black} & \text{if } (i \bmod 2) \neq (j \bmod 2) \end{cases} \tag{6.5}$$

The update to the electric potential is the same as in the standard Gauss-Seidel method[39].

$$V_{i,j}(t) = \frac{1}{4}\left[V_{i+1,j}(t) + V_{i,j+1}(t) + V_{i-1,j}(t) + V_{i,j-1}(t)\right] \tag{6.6}$$

However, due to the way sites are labeled and the form of this update, it can be seen that the updates for the Red sites depends only on the values of the potential on Black sites, and vice versa. Therefore, this update can be made fully explicit by alternating updating the Red sites and Black sites. The update schedule for updates n and $n+1$ is visualized in Fig. 6.2.

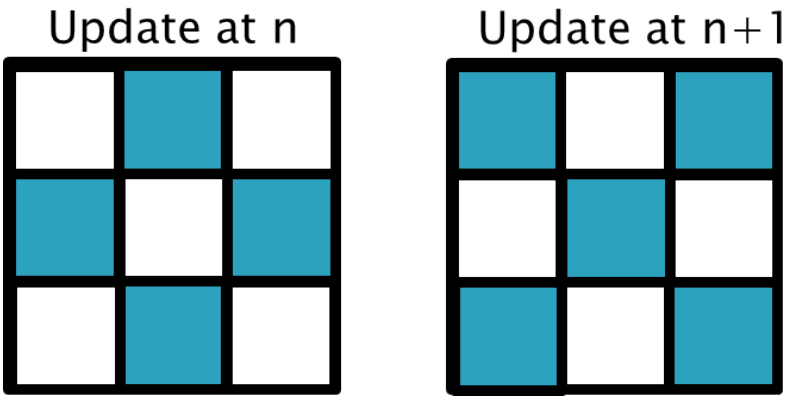

Figure 6.2: Updated lattice sites on the n^{th} iteration and the following iteration.

The relaxation algorithm proceeds in an alternating fashion by updating the Red sites and the Black sites until convergence. On each update, the electric potential at that site is set to be the average of the values of its neighboring sites.

As stated, this algorithm requires $\mathcal{O}(S^2)$ iterations to reduce the error in the computed electric potential by an order of magnitude[46]. This is impractical for the purpose at hand, but fortunately there exists a minor modification of the above algorithm that gives much faster convergence. If Eq. 6.6 is modified to read

$$V_{i,j}(t) = (1-\omega)\, V_{i,j}(t) + \frac{\omega}{4}\left[V_{i+1,j}(t) + V_{i,j+1}(t) + V_{i-1,j}(t) + V_{i,j-1}(t)\right] \tag{6.7}$$

then it can be shown that the number of iterations required to reduce the error in the electric potential is $\mathcal{O}(S)$ for the appropriate choice of the constant ω[46]. This is known as Successive Over-Relaxation (SOR). The optimal value of ω for a square grid is given by the equation

$$\omega = \frac{2}{1+\frac{\pi}{S}} \tag{6.8}$$

which evaluates to $\omega \approx 2$. This was the value used in previous work. With this value of ω, the number of iterations n_{10} required to reduce the error by an order of magnitude is

approximately

$$n_{10} \approx -\frac{1}{\log_{10}\left(1 - \frac{4\pi}{S+1}\right)} \tag{6.9}$$

For the value $S = 512$ this gives $n_{10} \approx 93$. To ensure convergence, the relaxation was run for $4 \times n_{10}$ iterations.

6.3.4 Interpolation scheme

The relaxation method described in section 6.3.3 gives an estimate of the potential $V_{i,j}(t)$ which is defined only on the discrete lattice points. For the calculation of the electric charge and forces, it is necessary to have an estimate of the potential $V^*(x, y, t)$, the numerical solution of Eq. 6.1, which is defined for all points in the region of interest. This can be computed by interpolation[44, 45] between the points of the discretized solution. Provided the potential is defined on all lattice points and is continuous in the regions between them, a bilinear interpolation can be used. After defining the scale $s \equiv \frac{S}{L}$ to be the number of lattice sites per cm, this is computed as follows

$$V^*(x, y, t) = [\lceil sx \rceil - sx, sx - \lfloor sx \rfloor] \begin{bmatrix} V_{\lfloor sx \rfloor, \lfloor sy \rfloor}(t) & V_{\lfloor sx \rfloor, \lceil sy \rceil}(t) \\ V_{\lceil sx \rceil, \lfloor sy \rfloor}(t) & V_{\lceil sx \rceil, \lceil sy \rceil}(t) \end{bmatrix} \begin{bmatrix} \lceil sy \rceil - y \\ y - \lfloor sy \rfloor \end{bmatrix} \tag{6.10}$$

This interpolation combined with the relaxation method allows for the calculation of the numerically evaluated potential for any point within the region of interest defined by $x, y \in (0, L)$.

6.4 Evaluation of Force and Charge surface integrals

With the numerical solution of Eq. 6.1 it is possible to evaluate the electrical force and total charge on each conductor as both quantities are related to surface integrals of derivatives of the electric potential. These surface integrals will be converted into sums over an idealized

surface that surrounds each conductor. This surface is centered on the conductor in question, and is composed of $N_{surf} = 500$ equally spaced points located at a distance of $R + \sqrt{2}\frac{L}{S}$ from the center. An idealized example of the integration surface with $N_{surf} = 8$ sites can be seen in Fig. 6.3.

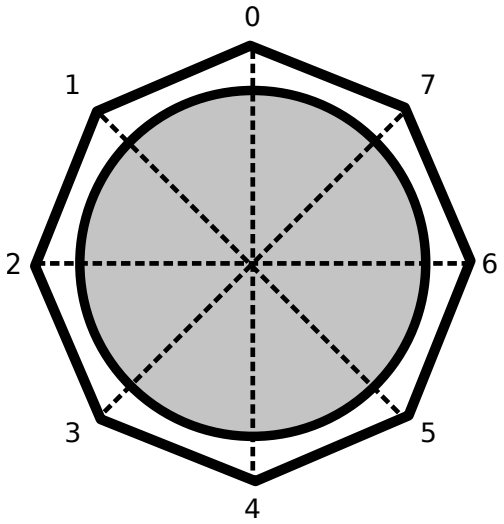

Figure 6.3: Illustration of the integration surface for eight surface sites

Both the charge and the force integrals will be computed over these surfaces. For conductor i which has its center at (x_i, y_i), the coordinates (x_{ij}, y_{ij}) of the j^{th} vertex on the integration surface are

$$\begin{aligned} x_{ij} &= x_i + \left(R + \sqrt{2}\frac{L}{S}\right)\cos\left(\frac{2\pi j}{N_{surf}}\right) \\ y_{ij} &= y_i + \left(R + \sqrt{2}\frac{L}{S}\right)\sin\left(\frac{2\pi j}{N_{surf}}\right) \end{aligned} \tag{6.11}$$

The surface normal vector at the j^{th} is

$$\hat{n}_{ij} = \sin\left(\frac{2\pi j}{N_{surf}}\right)\hat{x} - \cos\left(\frac{2\pi j}{N_{surf}}\right)\hat{y} \tag{6.12}$$

Each surface segment has the same total length of $\Delta s = \frac{2\pi R}{N_{surf}} + \frac{\sqrt{2}L}{N_{surf}S}$ Both the force and charge integrals depend on the gradient of the electric potential, which can be computed

from the interpolation given in Eq. 6.10. The components of the gradient are as follows

$$\begin{aligned}\frac{\partial V^*(x,y,t)}{\partial x} &= \left(-V_{\lfloor sx\rfloor,\lfloor sy\rfloor}(t) + V_{\lceil sx\rceil,\lfloor sy\rfloor}(t)\right)(\lceil y\rceil - y) \\ &\quad + \left(-V_{\lfloor sx\rfloor,\lceil sy\rceil}(t) + V_{\lceil sx\rceil,\lceil sy\rceil}(t)\right)(y - \lfloor y\rfloor) \\ \frac{\partial V^*(x,y,t)}{\partial y} &= \left(V_{\lfloor sx\rfloor,\lceil sy\rceil}(t) - V_{\lfloor sx\rfloor,\lfloor sy\rfloor}(t)\right)(\lceil x\rceil - x) \\ &\quad + \left(V_{\lceil sx\rceil,\lceil sy\rceil}(t) + V_{\lceil sx\rceil,\lfloor sy\rfloor}(t)\right)(x - \lfloor x\rfloor)\end{aligned} \tag{6.13}$$

And of course the gradient is then

$$\vec{\nabla} V^*(x,y,t) = \frac{\partial V^*(x,y,t)}{\partial x}\hat{x} + \frac{V^*(x,y,t)}{\partial y}\hat{y} \tag{6.14}$$

From this the derivative with respect to the normal direction of the integration surface can be calculated using the following equation.

$$\left.\frac{\partial V^*(x,y,t)}{\partial \hat{n}_i}\right|_{(x_{ij},y_{ij})} = \frac{\partial V^*(x_{ij},y_{ij},t)}{\partial x}\sin\left(\frac{2\pi j}{s}\right)\hat{x} - \frac{\partial V^*(x_{ij},y_{ij},t)}{\partial y}\cos\left(\frac{2\pi j}{s}\right)\hat{y} \tag{6.15}$$

This is the quantity which is needed for the calculation of the electric force and charge.

6.4.1 Numeric integration for electric force

In terms of the numerically calculated potential from Eq. 6.10, the surface integral for the electrostatic force can be written

$$\vec{F}_i = \frac{\epsilon}{2}\int_{\partial\Omega_i}\left(\frac{V^*(x,y,t)}{\partial \hat{n}_i}\right)^2 \hat{n}_i \partial\Omega_i \tag{6.16}$$

With Eq. 6.15, the integrand can be evaluated numerically. Because the surface of integration is closed, the trapezoid method[47] gives accuracy to order $\mathcal{O}\left(N_{surf}^{-3}\right)$ and is quickly

computed. The force integral then becomes two sums, one for each component. They are

$$\begin{aligned} F_{ix} &= \left(\frac{2\pi R}{N_{surf}} + \frac{\sqrt{2}L}{N_{surf}S}\right) \sum_{j=0}^{N_{surf}} \left(\left.\frac{\partial V^*(x,y,t)}{\partial \hat{n}_i}\right|_{(x_{ij},y_{ij})}\right)^2 \hat{x} \\ F_{iy} &= \left(\frac{2\pi R}{N_{surf}} + \frac{\sqrt{2}L}{N_{surf}S}\right) \sum_{j=0}^{N_{surf}} \left(\left.\frac{\partial V^*(x,y,t)}{\partial \hat{n}_i}\right|_{(x_{ij},y_{ij})}\right)^2 \hat{y} \end{aligned} \tag{6.17}$$

Thus the electrostatic force on each conductor can be computed numerically from the potential from section 6.3.4.

6.4.2 Numeric integration for conductor charge

The evaluation is slightly simpler for the case of the electric charge. The integral can be written as

$$Q_i = -\epsilon \int_{\partial\Omega_i} \frac{\partial V^*(x,y,t)}{\partial \hat{n}_i} \partial\Omega_i \tag{6.18}$$

Once again, using the trapezoid rule, this can be approximated as a sum over the integration surface

$$Q_i = \left(\frac{2\pi R}{N_{surf}} + \frac{\sqrt{2}L}{N_{surf}S}\right) \sum_{j=0}^{N_{surf}} \left(\hat{n}_i \cdot \vec{\nabla} V^*(x,y,t)\Big|_{(x_{ij},y_{ij})}\right)^2 \tag{6.19}$$

The charge computed from the numerically calculated potential will be used to compute the correct boundary conditions in section 6.5.

6.5 Computing the electrostatic boundary conditions

While the relaxation method in section 6.3.3 works by solving Eq. 6.1 in the case where the potential on the surface of each conducting particle is known, this quantity is actually quite difficult to work with. This is due to the fact that a change in the position of one conductor affects the electric potential on every other conductor in the system. The electric charge Q_i on conductor i is related to the electric potential ϕ_j on every conductor from $j = 1$ to $j = N$

by the capacitance matrix.

$$Q_i = \sum_{j=1}^{N} \mathcal{C}_{ij}\phi_j \tag{6.20}$$

However, the charge on conductor i does not change if conductor j is moved, as it is an intrinsic property of conductor i. This presents a problem in that the configuration of the system is most easily expressed in terms of this electric charge, but solutions to Eq. 6.1 are most easily found in terms of electric potential. The goal then is to convert knowledge of the electric charge and position of each conductor into knowledge of the electric potential of each conductor such that the solution of Eq. 6.1 can be found.

This is done via an iterative procedure in which an initial estimate $\phi^*_{i=1,2,...,N}$ for the electric potential on each conductor is refined to be closer to the true values $\phi_{i=1,2,...,N}$.

6.5.1 Total error in conductor potentials

In order to iteratively improve the estimate of the conductor potentials, the error in the current estimate must be defined. With the current estimates $\phi^*_{i=1,2,...,N}$, it is possible to calculate the inferred charges $Q^*_{i=1,2,...,N}$ that occur on each conductor. This is done by using the ϕ^*'s as the boundary conditions for the method in section 6.2 to calculate the electric potential in the region of interest followed by using the method in section 6.4 to evaluate the charge on the conductors. A reasonable choice for the $\phi^*_i(t)$'s is simply the value of the conductor potentials on the previous time step

$$\phi^*_i(t) = \phi_i(t - \Delta t) \tag{6.21}$$

The Q^*_i's are therefore functions of the estimate of the conductor potentials and can be written $Q^*_i\left(\phi^*_1, \phi^*_2, ..., \phi^*_N\right)$.

With the Q^*_i's calculated, the total error associated with taking the ϕ^* potentials as

boundary conditions is defined to be the sum of squared errors (SSE) for each conductor.

$$\mathcal{E}\left(\phi_1^*, \phi_2^*, ..., \phi_N^*\right) = \frac{1}{2}\sum_{i=1}^{N}\left(Q_i - Q_i^*\left(\phi_1^*, \phi_2^*, ..., \phi_N^*\right)\right)^2 \tag{6.22}$$

By the uniqueness property of solutions to Eq. 6.1 there is only one solution which has $\mathcal{E}\left(\phi_1^*, \phi_2^*, ..., \phi_N^*\right) = 0$. Therefore, finding the correct conductor potentials $\phi^*_{i=1,2,...,N}$ is equivalent to finding the roots of Eq. 6.22.

Furthermore, it can be shown that this function only has one minimum that corresponds to the solution with $\mathcal{E}\left(\phi_1^*, \phi_2^*, ..., \phi_N^*\right) = 0$. This can be seen by evaluating the derivative of the total error:

$$\frac{\partial \mathcal{E}}{\partial \phi_i^*} = -\sum_{j=1}^{N}\left(Q_j - Q_j^*\left(\phi_1^*, \phi_2^*, ..., \phi_N^*\right)\right)\mathcal{C}_{ij} \tag{6.23}$$

where $\mathcal{E} = \mathcal{E}\left(\phi_1^*, \phi_2^*, ..., \phi_N^*\right)$. Here Eq. 6.20 has been used, along with the fact that the capacitance matrix is symmetric[48, 49]. Extrema of the error function in Eq. 6.22 must have $\frac{\partial \mathcal{E}}{\partial \phi_i^*} = 0$, or

$$\sum_{j=1}^{N}\mathcal{C}_{ij}\left(Q_j - Q_j^*\left(\phi_1^*, \phi_2^*, ..., \phi_N^*\right)\right) = 0 \tag{6.24}$$

However, because the capacitance matrix is invertible, the only solution must have

$$\left(Q_i - Q_i^*\left(\phi_1^*, \phi_2^*, ..., \phi_N^*\right)\right) = 0 \qquad \forall i \in \{1, 2, ..., N\} \tag{6.25}$$

Thus the only minumum of Eq. 6.22 is the desired solution.

6.5.2 Error minimization by approximate gradient descent

Since the error defined in Eq. 6.22 has only one minimum corresponding to the desired conductor potentials, gradient descent can be used to compute the potentials. Gradient

descent for this problem involves making the update

$$\phi_i^{*(n+1)} = \phi_i^{*(n)} - \eta \frac{\partial \mathcal{E}^{(n)}}{\partial \phi_i^{*n}} \tag{6.26}$$

where η is some small positive constant. On the n^{th} iteration, the derivative of the error can be written as

$$\frac{\partial \mathcal{E}^{(n)}}{\partial \phi_i^{*n}} = -\sum_{j=1}^{N} \left(Q_j - Q_j^* \left(\phi_1^{*n}, \phi_2^{*n}, ..., \phi_N^{*n}\right)\right) \mathcal{C}_{ij} \tag{6.27}$$

The full gradient descent update is then

$$\phi_i^{*(n+1)} = \phi_i^{*(n)} + \eta \sum_{j=1}^{N} \left(Q_j - Q_j^* \left(\phi_1^*, \phi_2^*, ..., \phi_N^*\right)\right) \mathcal{C}_{ij} \tag{6.28}$$

However, this is still an impractical update as it requires knowledge of the entire capacitance matrix. Instead, it is possible to consider making a simplified update by considering only the diagonal terms of the capacitance matrix. This is the approximation

$$\frac{\partial \mathcal{E}^{(n)}}{\partial \phi_i^{*n}} \approx -\left(Q_j - Q_j^* \left(\phi_1^*, \phi_2^*, ..., \phi_N^*\right)\right) \mathcal{C}_{ii} \tag{6.29}$$

Since $\mathcal{C}_{ii}$ is always positive[48, 49], we can absorb this into the constant η by setting $\eta \to \mathcal{C}_{ii}\eta$ This gives the approximate gradient descent update

$$\phi_i^{*(n+1)} = \phi_i^{*(n)} + \eta \left(Q_j - Q_j^* \left(\phi_1^*, \phi_2^*, ..., \phi_N^*\right)\right) \tag{6.30}$$

This update can be computed directly using only the quantities computed in section 6.5.1.

6.5.3 Proof of convergence

While the update proposed in Eq. 6.30 is straightforward to calculate, it is not obvious that it converges on the correct solution. Convergence can be proven by considering the change

in error over one iteration

$$\Delta\mathcal{E}^{(n+1)} = \mathcal{E}^{(n+1)} - \mathcal{E}^{(n)} \tag{6.31}$$

From now on the shorthand $q_i^{(n)} \equiv \left(Q_i - Q_i^* \left(\phi_1^{*(n)}, \phi_2^{*(n)}, ..., \phi_N^{*(n)}\right)\right)$ will be used. In terms of this quantity, the change in error after one iteration is

$$\Delta\mathcal{E}^{(n+1)} = \frac{1}{2}\sum_{i=1}^{N}\left(q_i^{(n)} + \eta\sum_{j=1}^{N}\left(\mathcal{C}_{ij}q_j^{(n)}\right)\right)^2 - \frac{1}{2}\sum_{i=1}^{N}\left(q_i^{(n)}\right)^2 \tag{6.32}$$

This can be simplified into a more useful form

$$\Delta\mathcal{E}^{(n+1)} = \frac{\eta^2}{2}\sum_{i=1}^{N}\left[\sum_{j=1}^{N}\mathcal{C}_{ij}q_j^{(n)}\right]^2 - \eta\sum_{i=1}^{N}\sum_{j=1}^{N}q_i^{(n)}\mathcal{C}_{ij}q_j^{(n)} \tag{6.33}$$

While the term proportional to η^2 is always positive and has the potential to cause the error to increase, the term proportional to η is always negative. This follows from the fact that the capacitance matrix $\mathcal{C}_{ij}$ is always a positive matrix[48, 49]. Therefore, the error is always decreasing when $\mathcal{E}^{(n+1)} < 0$, or

$$\frac{\eta}{2}\sum_{i=1}^{N}\left[\sum_{j=1}^{N}\mathcal{C}_{ij}q_j^{(n)}\right]^2 < \sum_{i=1}^{N}\sum_{j=1}^{N}q_i^{(n)}\mathcal{C}_{ij}q_j^{(n)} \tag{6.34}$$

This gives the convergence requirement for the constant η. Defining the critical value of η

$$\eta_c = 2\frac{\sum_{i=1}^{N}\sum_{j=1}^{N}q_i^{(n)}\mathcal{C}_{ij}q_j^{(n)}}{\sum_{i=1}^{N}\left[\sum_{j=1}^{N}\mathcal{C}_{ij}q_j^{(n)}\right]^2} \tag{6.35}$$

the error in the estimate of the conductor potentials is always decreasing provided that η is chosen such that $\eta < \eta_c$.

Furthermore, it is possible to show that the value of η_c is non-zero except in the trivial case. It is clear that the only possible scenario in which $\eta_c = 0$, is one in which $q_i^{(n)} = 0$ for all i as well. This occurs when the estimates for the conductor potentials are near their

correct values. Taking the limit of η_c as the solution is approached gives, after multiple uses of L'Hospital's rule

$$\begin{aligned}
\lim_{q_k^{(n)}\to 0} \eta_c &= \lim_{q_k^{(n)}\to 0} \frac{\sum_{i=1}^{N}\sum_{j=1}^{N}\left(\delta_{ik}\mathcal{C}_{ij}q_j^{(n)} + q_i^{(n)}\mathcal{C}_{ij}\delta_{jk}\right)}{\sum_{i=1}^{N}\left[\sum_{j=1}^{N}\mathcal{C}_{ij}q_j^{(n)}\right]\sum_{j=1}^{N}\mathcal{C}_{ij}\delta_{jk}} \\
&= \lim_{q_k^{(n)}\to 0} \frac{2\sum_{i=1}^{N}\mathcal{C}_{ki}q_i^{(n)}}{\sum_{i=1}^{N}\sum_{j=1}^{N}\mathcal{C}_{ik}\mathcal{C}_{ij}q_j^{(n)}} \\
&= \lim_{q_k^{(n)}\to 0} \frac{2\sum_{i=1}^{N}\mathcal{C}_{ik}\delta_{ik}}{\sum_{i=1}^{N}\sum_{j=1}^{N}\mathcal{C}_{ik}\mathcal{C}_{ij}\delta_{jk}} \\
&= \frac{2\mathcal{C}_{kk}}{\sum_{i=1}^{N}\mathcal{C}_{ik}^2}
\end{aligned} \tag{6.36}$$

Once again, following from the fact that the capacitance matrix is positive[48, 49], this shows that even as the solution is approached there is always a non-zero value for η that causes the error to decrease. The convergence behavior of this update is governed by the conductors with smallest self capacitance in the system.

6.5.4 Results for two conductors

To test the implementation of the above algorithm for evaluating the potentials of conductors held at a known charge, it was applied to the known case of two circular objects in 2D space. This system has the analytical solution for the capacitance C in terms of the object radius R and the distance between their centers d. In non-dimensional form, this is given by

$$\frac{C}{\epsilon} = \frac{\pi}{\cosh^{-1}\left(\frac{d}{2R}\right)} \tag{6.37}$$

The first object was held at a potential $\phi_1 = 0$ while the second object was constrained to have a total charge $Q_2 = 1\ sC$. A diagram of the configuration can be seen in Fig. 6.4

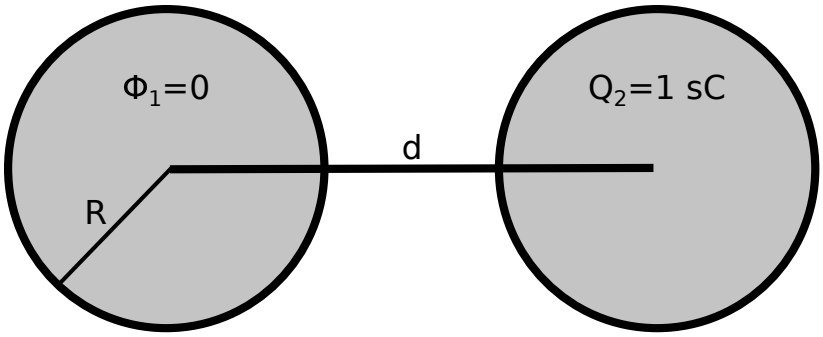

Figure 6.4: Configuration of two circular wires

The algorithm as described above was used to evaluate the potential ϕ_2 on the second object, and the capacitance was computed via $C = Q_2/\phi_2$ for several values of the ratio $\frac{d}{R}$. A constant value of $\eta = 0.01$ was used in the update given by Eq. 6.30. Figure 6.5 shows the numerical result compared to the known theoretical result. The numerical result is a near exact match to the theoretical result.

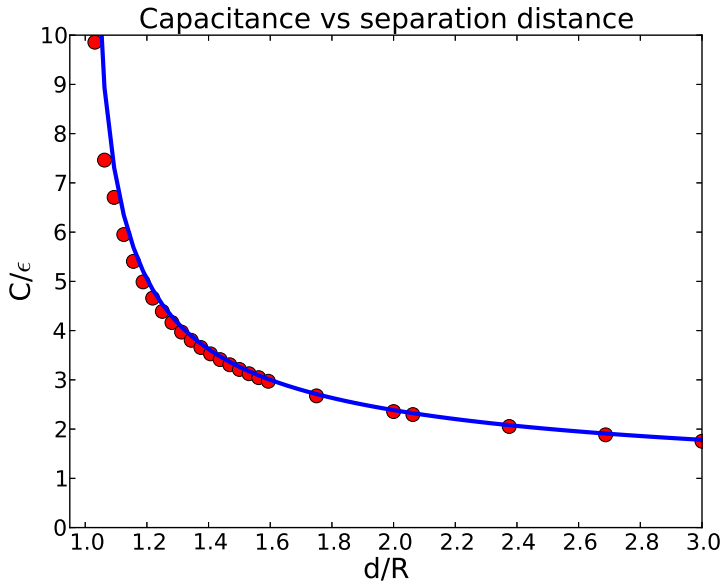

Figure 6.5: Computed capacitance (red dots) as compared to theoretical value from Eq. 6.37 (blue line)

It is also informative to check the rate at which the error is reduced. For the two circular objects, figure 6.6 shows the error as computed with Eq. 6.22 as a function of the number

of iterations of Eq. 6.30 for $\frac{d}{2R} = 4$ and $\eta = 0.01$. The blue line is an exponential fit of the form

$$\mathcal{E}^{(n)} = \mathcal{E}^{(0)} e^{-\lambda n} \tag{6.38}$$

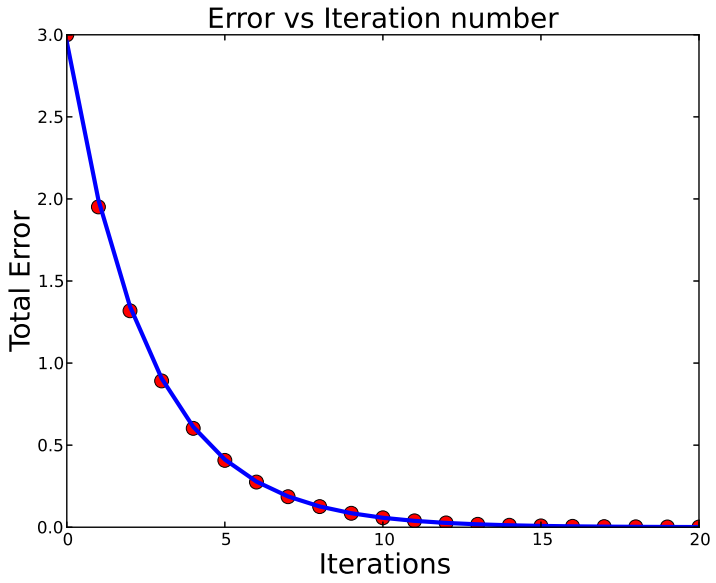

Figure 6.6: Total error as a function of number of iterations compared to an exponential fit as in Eq. 6.38

The total error decreases exponentially as the number of iterations increases. This is expected given the form of Eq. 6.33, which for the case of two objects, one of which held at $\phi_1 = 0$ reduces to

$$\begin{aligned} \Delta\mathcal{E}^{(n+1)} &= \frac{\eta^2}{2}\left(\mathcal{C}_{12}q_2^{(n)} + \mathcal{C}_{22}q_2^{(n)}\right)^2 - \eta\mathcal{C}_{22}\left(q_2^{(n)}\right)^2 \\ &\approx -2\eta\mathcal{C}_{22}\mathcal{E}^{(n)} \qquad \text{for} \quad \eta \ll 1 \end{aligned} \tag{6.39}$$

Not only does the error decrease as expected, it does so quickly. If the estimates of the conductor potentials are close to the correct values, only a few iterations of 6.30 may be required to achieve an acceptable total error.

6.6 Electronics of particle collions

Special care is required in the case where two or more conductors are in contact with one another. In this case, the machinery described above still works, but each group of conductors which are in contact must me considered as a single conducting object. This combined object will have a charge equal to the sum of the charges of its constituent conductors by conservation of charge. In addition, the constituent conductors will all have the same electric potential, as the combined conductor will form an equipotential surface. A diagram of how the electronic degrees of freedom behave during a collision between two objects can be seen in figure 6.7.

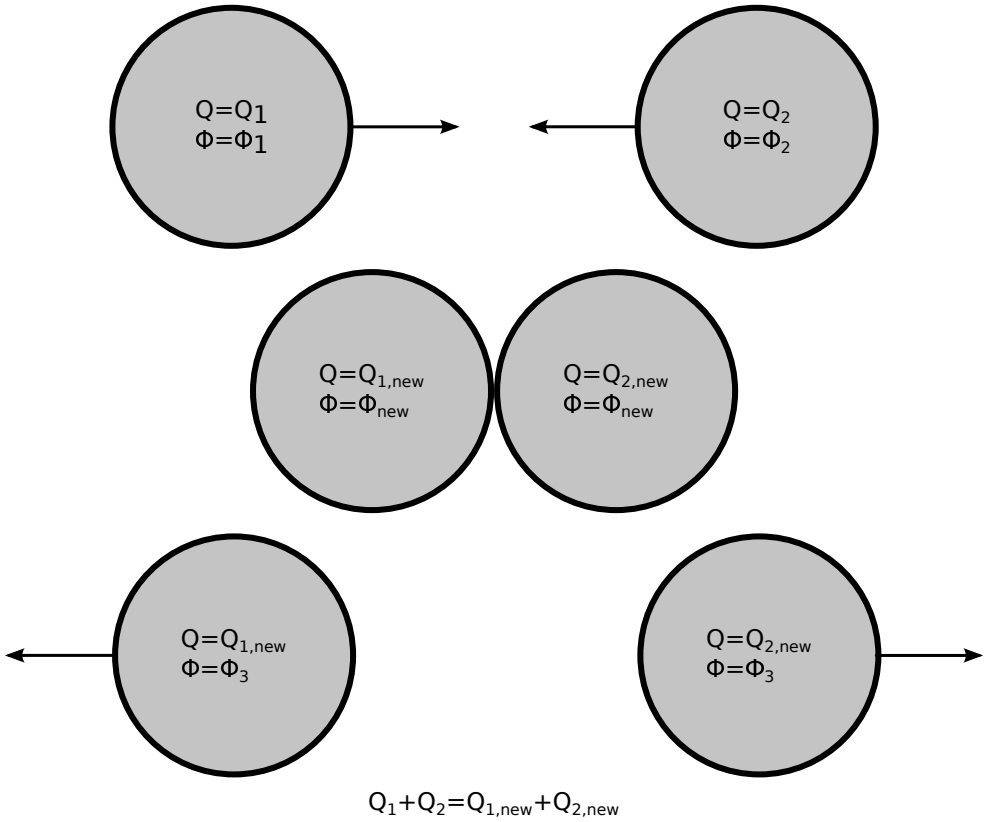

Figure 6.7: Diagram of the behavior of charge and potential during a collision between two conductors

Detecting combined conductors is done by first defining the id number of the combined conductor, α to be the minimum index of its constituent conductors. One way to accomplish

this is to have each particle carry an extra index that corresponds to the index of the combined conductor α that it belongs to. Then update that index to be the minimum index of the conductors it is in electrical contact with and repeat this process until no indices change. To carry out this procedure, a graph $\mathcal{G}(t)$ of electrical contacts must be defined. A connection of weight one between conductor i and j is said to exist if the distance between the two obeys

$$\sqrt{(x_i - x_j)^2 + (y_i - y_j)^2} < 3R \tag{6.40}$$

and no connection exists otherwise. By this definition, the trivial connection of a conductor to itself is permitted. Then the id of the combined conductor can be written as the recursive relation

$$\alpha_i = \min \alpha_j \qquad \forall \mathcal{G}_{ij}(t) = 1 \tag{6.41}$$

The recursion relation can be evaluated by initializing with $\alpha_i = i$ and iterating until none of the α_i's change. In the event that a conductor has no electrical contacts, this initialization ensures that the combined conductor it belongs to will have the id of the only conductor it contains. This uniquely defines the id of the combined conductor and specifies all individual conductors that belong to it.

Once the combined conductors have been assigned unique ids, the algorithm in section 6.5 can be applied to the combined conductors and their potentials. With the potentials of the combined conductors computed, the individual conductor potentials are also known as they have the same potential as the combined conductor they belong to. Additionally, the individual conductor charges can be computed as usual from Eq. 6.18. Through this procedure, the transfer of charge between conductors in contact is accounted for with minimal extra overhead, and the evolution of the electronic degrees of freedom in a collision between conductors is specified.

6.7 Integration of equations of motion

Once the electrostatic degrees of freedom have been solved, it is straightforward to integrate the equations of motion. The electrical force on each conductor is computed from Eq. 6.16, and so the positions, and so the positions and velocities of each conductor can be updated using Euler's method:

$$\begin{aligned}
x_i(t+\Delta t) &= x_i(t) + \frac{p_{x,i}(t)}{m_i}\Delta t \\
y_i(t+\Delta t) &= y_i(t) + \frac{p_{y,i}(t)}{m_i}\Delta t \\
p_{x,i}(t+\Delta t) &= p_{x,i}(t) + \left(F_i - \frac{\gamma_i}{m_i}p_{x,i}(t)\sum_{j\neq i}^{N} F_{contact}(\vec{r}_i - \vec{r}_j)\cdot\hat{x}\right)\Delta t \\
p_{y,i}(t+\Delta t) &= p_{y,i}(t) + \left(F_i - \frac{\gamma_i}{m_i}p_{y,i}(t) + \sum_{j\neq i}^{N} F_{contact}(\vec{r}_i - \vec{r}_j)\cdot\hat{y}\right)\Delta t
\end{aligned} \tag{6.42}$$

Here $F_{contact}$ is the contact force as defined in Eq. 5.9. The time step Δt used here was $\Delta t = 0.01ms$. A small time step is required to adequately resolve the mechanics of the conductor collisions generated by $F_{contact}$. Since recalculating the electric potential is an expensive operation and this quantity changes on a much longer timescale, this was done with a time step of $\Delta t = 1ms$.

Chapter 7

Analysis methods and results

7.1 Stationary state

The numerical procedure in Chapter 6 was iterated until a stationary state was achieved. In the stationary state (and in the absence of forces which were not considered in the model of Chapter 5), all particles are connected to the ground electrode and have the same surface potential. This in turn implies that the electrostatic forces due to effects internal to the system vanish, providing a stopping criterion for the numerical calculation. An example of the calculated stationary state compared to the experimental system can be seen in Figure 7.1.

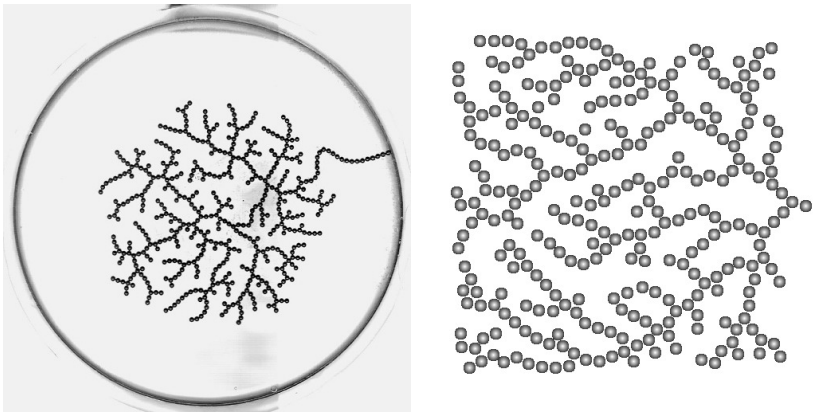

Figure 7.1: Stationary state reached for a system of $N = 324$ total conductors.

7.2 Definition of network graph

The $(x_i(t), y_i(t))$ positions of each of the $i \in \{1, ..., N\}$ conductors was saved for each time t that was evaluated from the numerical method described in chapter 6. From these, a graph representation of the state of the system was calculated as a function of time. In general, the network graph $\mathcal{G}(t)$ is planar, possibly contains many different sub-graphs, and consists of N nodes. The network graph is defined through its adjacency matrix w by assigning a weight $w_{i,j} = 1$ between two conductors i, j which are directly electrically connected and a weight of $w_{i,j} = 0$ when they are not. Two conductors are connected if

$$|\vec{r}_i(t) - \vec{r}_j(t)| < 3R \tag{7.1}$$

where $\vec{r}_i(t) = x_i(t)\hat{x} + y_i(t)\hat{y}$. This convention is identical to the one used in [3].

It is also possible to define an anti-arborescence $\mathcal{A}(t)$ which is rooted at the ground electrode. To do this, each conductor is assigned a direct successor D. These have the physical interpretation that the flow of charge in the network is directed from conductor i to its direct successor D_i. The successors can be computed iteratively by first requiring that all conductors which are directly electrically connected to the ground electrode have the ground electrode as their direct successor. Then in each subsequent iteration, the successor D_i of the i^{th} conductor is defined to be the nearest conductor that is connected to i and has a successor provided that i does not already have a successor. This process can be iterated until no new successors can be assigned.

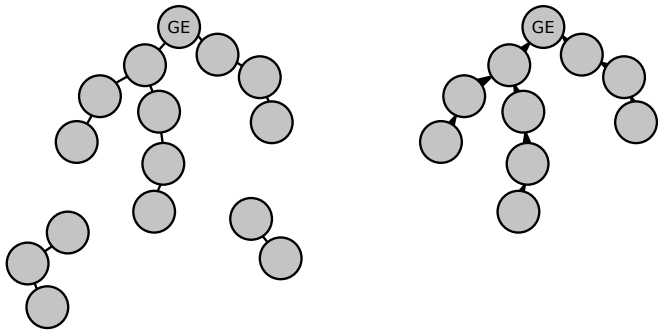

Figure 7.2: Left: Example network graph $\mathcal{G}$. Right: Example anti-arborescence $\mathcal{A}$ corresponding to the graph.

Depending on the connectivity of $\mathcal{G}$, it is possible that not all conductors are also in $\mathcal{A}$. Let M be the number or conductors in $\mathcal{A}$. By construction N is the number of conductors in $\mathcal{G}$, and so $M \leq N$. While $\mathcal{G}$ represents the electrical contacts between all conductors, $\mathcal{A}$ represents only the conductors which have a direct or indirect electrical path to the ground electrode. An example of the two types of graphs can be seen in figure 7.2.

7.3 Calculation of degree distribution

With the network graphs defined, relevant topological quantities can be calculated. First, the degree distribution of the graph $\mathcal{G}$ can be calculated from the adjacency matrix w. The degree d_i of a node i is defined by

$$d_i = \sum_{j=0}^{N} w_{ij} \tag{7.2}$$

Of specific interest is the total number of nodes of a given degree that have 'completed' a connection to the ground electrode. By construction, these are the nodes in $\mathcal{A}$, and so letting Δ_j be the total number of nodes of degree j:

$$\Delta_j = \sum_{i \in \mathcal{A}(t)} \delta_{j,d_i} \tag{7.3}$$

Where δ_{j,d_i} is the Kronecker delta between j and the degree of node i. The degree distribution for $\mathcal{A}$ is then defined by calling f_j the fraction of nodes of degree j:

$$f_j = \frac{\Delta_j}{M} \tag{7.4}$$

Another relevant quantity, the fraction of "branch" nodes which have more than two nodes directly connected to them, can be defined as

$$B = \frac{1}{M} \sum_{i>2} \Delta_i \tag{7.5}$$

7.3.1 Constraints on degree distribution

The fractions defined in Eq. 7.4 are not completely independent. First a normalization constraint of the form

$$\sum_{i=1}^{i_{max}} f_i = 1 \tag{7.6}$$

must be obeyed. Second, there is a constraint related to the number of branches and end-points. This can be interpreted as a statement that every branch in the tree $\mathcal{A}$ must have an end associated with it, and the number of branches created at a node of degree i is $i-2$. This constraint can be expressed in terms of the fractions f as

$$\sum_{i=1}^{i_{max}} (i-2) f_i + \frac{1}{N} = 0 \tag{7.7}$$

In the limit $N \gg 1$, the $1/N$ term may be dropped, and Eq. 7.6 and Eq. 7.7 can be combined to give

$$\sum_{i=1}^{i_{max}} i f_i = 2 \tag{7.8}$$

Eq. 7.8 implies that the average degree of nodes is $\langle i \rangle = 2$ for large N.

For spherical particles in 2D, the connection criterion of Eq.7.1 implies that the maximum

degree of any node is $i_{max} = 4$. Any node with a degree larger than this implies the presence of a closed loop in the network graph, which is forbidden as discussed in section **??**. Therefore the full degree distribution has four entries, but the above constrains reduce this to only two. Previously, the two quantities f_1 and B have been used to characterize the network topology [1, 3, 7]. Using $B = f_3 + f_4$, the degree distribution can be expressed as follows:

$$\begin{aligned} f_1 &= f_1 \\ f_2 &= 1 - (f_1 + B) \\ f_3 &= 2B - f_1 \\ f_4 &= f_1 - B \end{aligned} \tag{7.9}$$

7.4 Results for the degree distribution

Experimental results from [1] and [3] indicate that both the fraction of endpoints f_1 and the fraction of branch nodes B are constant regardless of network size. Specifically, it was found that $f_1 = 0.252$ and $B = 0.237$. These two quantities generate the full degree distribution

$$\begin{aligned} f_1 &= 0.252 \\ f_2 &= 0.511 \\ f_3 &= 0.222 \\ f_4 &= 0.015 \end{aligned} \tag{7.10}$$

This implies two relationships which are obeyed by networks of this type. First, there exists a linear relationship of the form

$$\Delta_1 (t \to \infty) = 0.252N \tag{7.11}$$

Second, there is another linear relation of the form

$$B\left(t \to \infty\right) = 0.237N \tag{7.12}$$

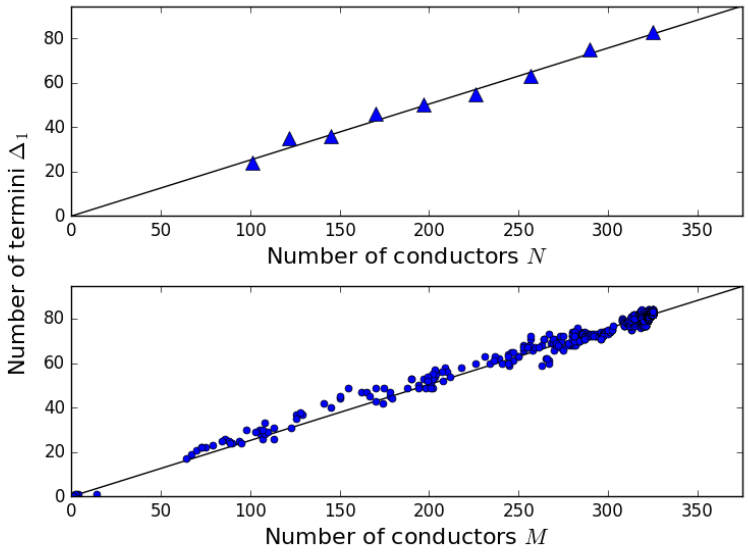

Figure 7.3: Top: Number of nodes Δ_1 which are endpoints (termini) as a function of N in the stationary state. Bottom: Number of nodes $\Delta_1(t)$ which are endpoints in the partially formed network $\mathcal{A}$. Solid lines in both plots show the experimental result $\Delta_1 = 0.252N$.

The top plot in Fig. 7.3 shows the experimentally measured result from Eq. 7.11 along with the results from the model defined in chapter 5 which were computed using the methods discussed in chapter 6 for a variety of network sizes N. Data in the top plot is taken after $t = 120s$, which is long enough for the network to have reached a stationary state.

In addition to this, the bottom plot of Fig. 7.3 shows a relationship similar to the one described in Eq. 7.11, but which holds for the network at all stages of formation. Concretely, this is the relationship

$$\Delta_1\left(t\right) = 0.252M(t) \tag{7.13}$$

Because M represents the number of conductors which have made a direct or indirect connection with the ground electrode, this relationship suggests that the fraction of endpoints in

the partially completed network is a constant. This behavior was reported for the first time in [7] and indicates previously unknown universal behavior in the approach to the steady state.

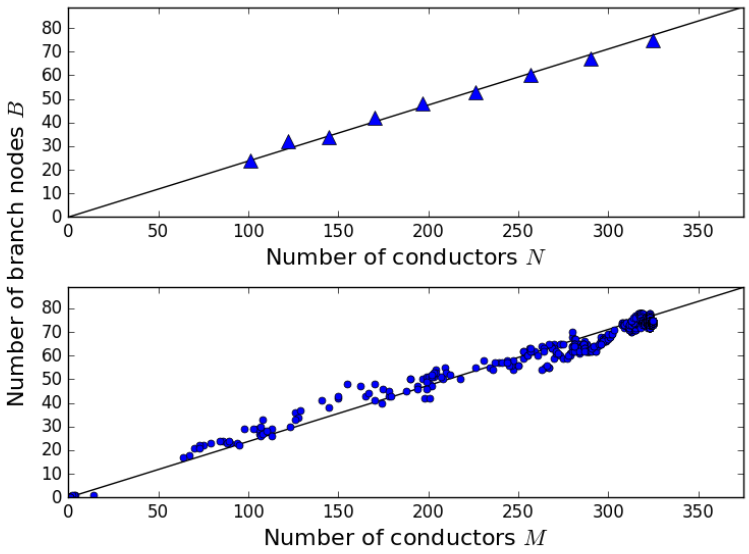

Figure 7.4: Top: Number of nodes B which are branch nodes as a function of N in the stationary state. Bottom: Number of nodes $B(t)$ which are endpoints in the partially formed network $\mathcal{A}$. Solid lines in both plots show the experimental result $B = 0.237N$.

The top plot in Fig. 7.4 shows a similar result for the numerically calculated number of branch nodes B after $t = 120s$ as compared to the experimental relation of Eq. 7.12. Again, the model as defined in chapter 5 and evaluated as in chapter 6 reproduces exactly the experimentally observed behavior.

Likewise, in the bottom plot of Fig. 7.4, it is also observed that the relationship

$$B(t) = 0.237M(t) \tag{7.14}$$

holds in the approach to the steady state as well. These results taken together require (through the constraints of Eq. 7.6 and Eq. 7.7) that the degree distribution of the drainage network which is connected to the ground electrode remain constant over time. However the

reason for this relationship is unknown, and seemingly indicates a global constraint on the network topology.

7.4.1 Connection to minimum spanning trees

The numerical degree distribution in Eq. 7.10 is known to be similar to the degree distribution found in other physical processes [27], such as diffusion limited aggregation (DLA). Of particular interest is the conjecture that this numerical degree distribution is identical to that of randomly generated minimum spanning trees in two dimensions.

A random minimum spanning tree of N nodes can be generated by the following procedure (Kruskal's algorithm [50]). First, a position (x_i, y_i) for each of the N nodes is randomly selected from a uniform distribution on the finite region $(x, y) \in [-1, 1]$. Define the weight w_{ij} of a hypothetical graph connection between node i and node j to be equal to the Euclidean distance between the nodes:

$$w_{ij} = \sqrt{(x_i - x_j)^2 + (y_i - y_j)^2} \tag{7.15}$$

Initialize the set $\mathcal{S}$ such that it contains all possible edges with $i < j$. Initialize the forest $\mathcal{F}$ to be the empty set. While there are still nodes which are not connected either directly or indirectly by the edges contained in $\mathcal{F}$, remove the edge $s \in \mathcal{S}$ from $\mathcal{S}$ which has the minimum weight w_{ij}. If the edge s connects two nodes which did not already have a direct or indirect connection via edges in $\mathcal{F}$, add this edge to $\mathcal{F}$. Repeat this process until all nodes are connected directly or indirectly by the edges contained in $\mathcal{F}$. At the end of this procedure, the edges in F define a tree with N nodes which has the property that the total sum of the weights (distance) between connected nodes is minimum. This type of tree is also known as a 2D Euclidean minimum spanning tree (EMST). An example of a tree generated with this procedure can be seen in Figure **??**

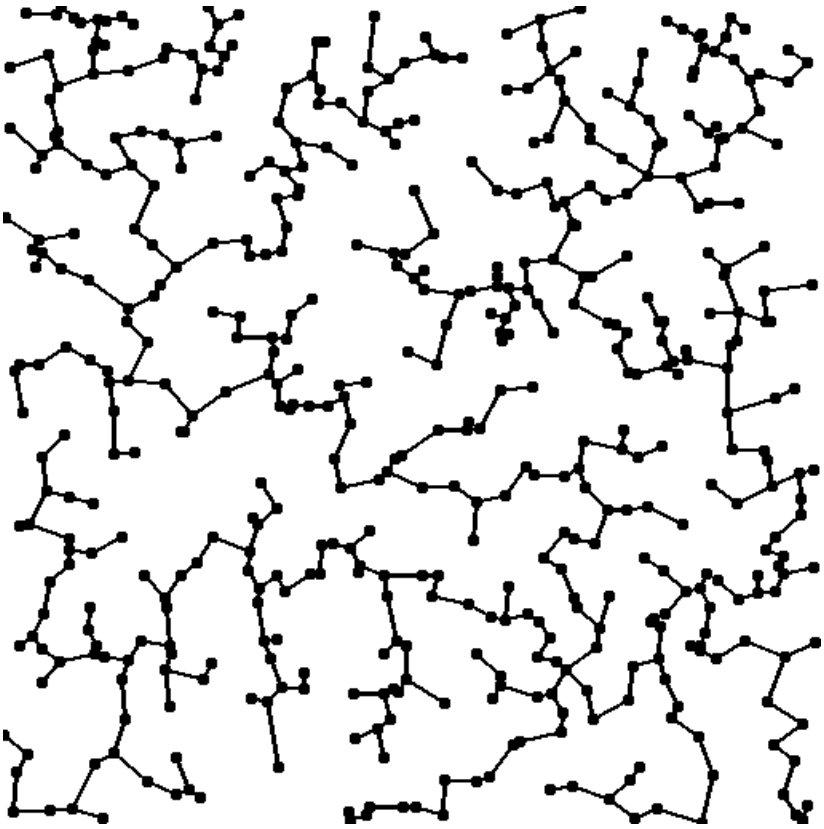

Figure 7.5: Euclidean minimum spanning tree generated from randomly distributed nodes in two dimensions.

The global constraint that the total weights of the connections is minimal makes this type of random tree difficult to analyze mathematically. However, it can be proved [51] that in the limit of large N, the degree distribution of EMSTs converges to a universal distribution. This distribution can be calculated numerically by randomly sampling EMSTs and computing their degree distributions[27]. This gives the numerical distribution for EMSTs as

$$\begin{aligned} f_1 &= 0.253 \pm 0.3 \\ f_2 &= 0.527 \pm 0.6 \\ f_3 &= 0.204 \pm 0.4 \\ f_4 &= 0.016 \pm 0.1 \end{aligned} \tag{7.16}$$

This is nearly an exact match to the degree distribution in Eq. 7.10.

7.5 Calculation of Strahler distribution

In addition to examining the degree distribution, it is also possible to probe the branching complexity of the network by making use of the directed nature of the tree $\mathcal{A}(t)$. This can be examined by computing quantities related to the Strahler numberings of the nodes in the graph, and compared to existing experimental results from a variety of systems including the one of interest[52, 53, 54]. The Strahler numbers $\mathcal{S}_i$ of each node can be calculated using the directed connections as defined successors D_i by the following procedure. First, a number of $\mathcal{S}_i = 1$ is assigned to all of the nodes $i \in \mathcal{A}$ which have $d_i = 1$. Then, for each of the nodes $j \in \mathcal{A}$ that do not have a Strahler number defined, $\mathcal{S}_j$ is set to be the maximum Strahler number of all the nodes which have node j as their direct successor. If more than one of these nodes has the maximum Strahler number, $\mathcal{S}_j$ is incremented by $\mathcal{S}_j \to \mathcal{S}_j + 1$. This procedure can be applied until all nodes have a Strahler number. The branching complexity of the network can then be understood by computing distribution of Strahler numbers as defined by

$$\sigma_j = \sum_{i \in \mathcal{A}(t)} \delta_{j,\mathcal{S}_i} \tag{7.17}$$

Where $\delta_{i,j}$ is the Kronecker delta.

7.6 Results for the Strahler distribution

An experimental relationship exists between the Strahler distribution and the size of the network[3]. These relationships follow a similar (linear) form as those discussed in Section 7.4 for the first three numbers in the Strahler distribution of Eq 7.17 and are as follows:

$$\begin{aligned} \sigma_1 &= 0.455N \\ \sigma_2 &= 0.275N \\ \sigma_3 &= 0.169N \end{aligned} \tag{7.18}$$

The linear relationships between the Strahler distribution and the size of the network are also known in the analysis of river (drainage) networks as Horton's laws[52]. These relationships can be seen in Figure 7.6.

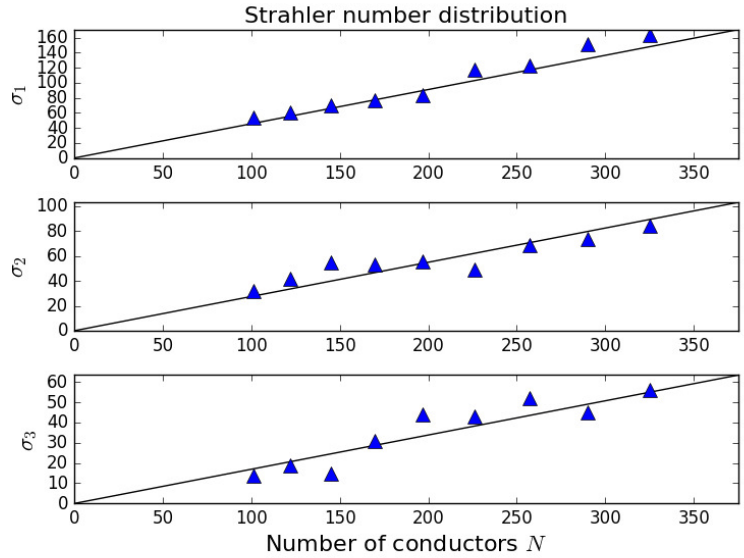

Figure 7.6: Experimental results (diagonal line) for the Strahler distribution as a function of network size $M(t)$. Blue dots show the numerically computed results from a single trial with $N = 324$.

Intuitively, these relationships suggest that the branching complexity of the stationary state does not vary with the size of the network. When taken together with the (time depenent) results from section 7.4, it appears as if the system approaches the stationary state by passing through a sequence of states which are not topologically distinct from the final stationary state.

Chapter 8

Conclusion

In this work, a first principles model of self-organizing particle wire networks has been developed. To this end, several experiments were carried out to determine the charge transport properties of single particles in strong electric fields as well as the stability properties of individual self-organized wires. These results informed the relevant physical effects that were included in the full model of the self-organization process. As specified, for more than a small number of conducting particles, the complex non-linear interactions necessary to capture the process present a considerable challenge in calculating model predictions. A large part of this difficulty stems from the dependence of the coefficients of capacitance on the dynamic configuration of the conductors in the system.

This difficulty is then overcome by a novel procedure that sidesteps the role of the capacitance coefficients in numerically solving the equations of motion. This makes the numerical solution of the model tractable for a large number of conductors on inexpensive hardware. After first proving that this procedure converges on the correct solution, and evaluating its effectiveness on a system with a known solution, it is applied to the full system, and demonstrated via a direct numerical integration of the equations of motion of the system.

Results from the model are found to agree with the experimentally obtained results nearly exactly. Specifically, the topology of the networks produced by numerically solving the model matches that of the experimental system as measured by the degree distribution of nodes and the distribution of Strahler numbers. An exciting new result is found in that it appears that all these topological quantities of the self-organized networks are constant

over all stages of the formation process. While experiments have not yet been carried out to verify this result, it is an interesting area of potential work.

While the majority of work presented here is aimed at modelling a specific set of conditions in which the self-organization occurs, namely that in which charge is added to a two dimensional region containing the particles, many of the methods developed here are applicable to other conditions as well. Of particular interest would be an application of this model to the scenario in which conducting wires are grown between two electrodes which are possibly in series with a resistor. Additionally, the model currently neglects the resistivity of the conducting particles. While this value is typically negligible in the scenario studied in this work, inclusion of this effect would allow more precise description of the steady state in other circumstances, and allow for more accurate characterization of the power dissipation dynamics. While these are not major changes from the model presented here, this would permit detailed study of the stability and entropy production of the resultant structures. The methods developed here both provide the necessary physical effects to model this phenomenon, as well as the tools required to extract numerical predictions of this self-organizing system.

References

[1] J. K. Jun and A. H. Hübler, "Formation and structure of ramified charge transportation networks in an electromechanical system," *Proceedings of the National Academy of Sciences of the United States of America*, vol. 102, no. 3, pp. 536–540, 2005.

[2] A. Belkin, A. Hubler, and A. Bezryadin, "Self-assembled wiggling nano-structures and the principle of maximum entropy production," *Scientific reports*, vol. 5, p. 8323, 2015.

[3] V. H. Soni, P. M. Ketisch, J. D. Rodríguez, A. Shpunt, and A. W. Hübler, "Topological similarities in electrical and hydrological drainage networks," 2011.

[4] A. Bezryadin, R. Westervelt, and M. Tinkham, "Self-assembled chains of graphitized carbon nanoparticles," *Applied physics letters*, vol. 74, no. 18, pp. 2699–2701, 1999.

[5] M. Dueweke, U. Dierker, and A. Hübler, "Self-assembling electrical connections based on the principle of minimum resistance," *Physical Review E*, vol. 54, no. 1, p. 496, 1996.

[6] C. Stephenson and A. Hubler, "Stability and conductivity of self assembled wires in a transverse electric field," *Scientific reports*, vol. 5, p. 15044, 2015.

[7] C. Stephenson, D. Lyon, and A. Hübler, "Topological properties of a self-assembled electrical network via ab initio calculation," *Scientific Reports*, vol. 7, 2017.

[8] J. W. Gibbs, *Elementary principles in statistical mechanics*. Courier Corporation, 2014.

[9] J. D. Stephenson and G. Reistad, "Analysis of a wood-fueled trimburner system for use in a combined-cycle, wood-fired power plant," *Journal of solar energy engineering*, vol. 110, no. 2, pp. 82–89, 1988.

[10] E. T. Jaynes, "Information theory and statistical mechanics," *Physical review*, vol. 106, no. 4, p. 620, 1957.

[11] E. T. Jaynes, "Information theory and statistical mechanics. ii," *Physical review*, vol. 108, no. 2, p. 171, 1957.

[12] C. E. Shannon, "A mathematical theory of communication, part i, part ii," *Bell Syst. Tech. J.*, vol. 27, pp. 623–656, 1948.

[13] E. T. Jaynes, "The minimum entropy production principle," *Annual Review of Physical Chemistry*, vol. 31, no. 1, pp. 579–601, 1980.

[14] I. Prigogine, "Time, structure, and fluctuations," *Science*, pp. 777–785, 1978.

[15] L. Onsager, "Reciprocal relations in irreversible processes. i.," *Physical review*, vol. 37, no. 4, p. 405, 1931.

[16] L. Onsager, "Reciprocal relations in irreversible processes. ii.," *Physical review*, vol. 38, no. 12, p. 2265, 1931.

[17] D. G. Miller, "Thermodynamics of irreversible processes. the experimental verification of the onsager reciprocal relations.," *Chemical Reviews*, vol. 60, no. 1, pp. 15–37, 1960.

[18] S. R. De Groot and P. Mazur, *Non-equilibrium thermodynamics*. Courier Corporation, 2013.

[19] G. Nicolis, I. Prigogine, *et al.*, *Self-organization in nonequilibrium systems*, vol. 191977. Wiley, New York, 1977.

[20] Y. Sawada, "A thermodynamic variational principle in nonlinear non-equilibrium phenomena," *Progress of Theoretical Physics*, vol. 66, no. 1, pp. 68–76, 1981.

[21] G. W. Paltridge, "Climate and thermodynamic systems of maximum dissipation," *Nature*, vol. 279, no. 5714, pp. 630–631, 1979.

[22] H. Ziegler, "Progress in solid mechanics," *Ed. Sneddon, IN y Hill, R., Nueva York (EE. UU.)(4)*, 1963.

[23] H. Ziegler and C. Wehrli, "On a principle of maximal rate of entropy production," *Journal of Non-Equilibrium Thermodynamics*, vol. 12, no. 3, pp. 229–244, 1987.

[24] L. Martyushev and V. Seleznev, "Maximum entropy production principle in physics, chemistry and biology," *Physics reports*, vol. 426, no. 1, pp. 1–45, 2006.

[25] M. Polettini, "Fact-checking zieglers maximum entropy production principle beyond the linear regime and towards steady states," *Entropy*, vol. 15, no. 7, pp. 2570–2584, 2013.

[26] G. Kirchhoff, "Ueber die anwendbarkeit der formeln für die intensitäten der galvanischen ströme in einem systeme linearer leiter auf systeme, die zum theil aus nicht linearen leitern bestehen," *Annalen der Physik*, vol. 151, no. 10, pp. 189–205, 1848.

[27] P. M. Ketisch, J. D. Rodrıguez, and A. W. Hübler, "Modeling the degree distribution of a fractal transportation network with a minimum spanning tree graph," *Department of Physics, University of Illinois at Urbana-Champaign, Urbana, Illinois*, 2008.

[28] L. Gorelik, A. Isacsson, M. Voinova, B. Kasemo, R. Shekhter, and M. Jonson, "Shuttle mechanism for charge transfer in coulomb blockade nanostructures," *Physical review letters*, vol. 80, no. 20, p. 4526, 1998.

[29] J. Lekner, "Electrostatics of two charged conducting spheres," in *Proc. R. Soc. A*, p. rspa20120133, The Royal Society, 2012.

[30] P. Glansdorff and I. Prigogine, "Structure, stability and fluctuations," *New York, NY: Interscience*, 1971.

[31] B. V. Mirtich, *Impulse-based dynamic simulation of rigid body systems*. University of California, Berkeley, 1996.

[32] G. Batchelor, "An introduction to fluid mechanics, 615 pp," *Cambridge University Press, New York*, 1967.

[33] D. A. Hanaor, Y. Gan, and I. Einav, "Contact mechanics of fractal surfaces by spline assisted discretisation," *International Journal of Solids and Structures*, vol. 59, pp. 121–131, 2015.

[34] E. Murphy and S. Morgan, "The dielectric properties of insulating materials," *Bell Labs Technical Journal*, vol. 16, no. 4, pp. 493–512, 1937.

[35] I. Abdelraziq and T. Nierat, "Rheology properties of castor oil: Temperature and shear rate-dependence of castor oil shear stress," *J Material Sci Eng*, vol. 5, no. 220, pp. 2169–0022, 2015.

[36] G. Elert, "The physics factbook: Density of steel," 2004.

[37] W. D. Callister and D. G. Rethwisch, *Materials science and engineering*, vol. 5. John Wiley & Sons NY, 2011.

[38] Nvidia, "Parallel programming and computing platform." `http://www.nvidia.com/object/cuda_home_new.html`.

[39] Y. Saad, "Parallel iterative methods for sparse linear systems," *Studies in Computational Mathematics*, vol. 8, pp. 423–440, 2001.

[40] L. Adams and J. Ortega, "A multi-color sor method for parallel computation," in *ICPP*, pp. 53–56, Citeseer, 1982.

[41] C. H. Rycroft, "Iterative methods for linear systems," *School of Engineering and Applied Sciences*, 2007.

[42] A. Gourlay, "Hopscotch: a fast second-order partial differential equation solver," *IMA Journal of Applied Mathematics*, vol. 6, no. 4, pp. 375–390, 1970.

[43] A. Gourlay and G. McGuire, "General hopscotch algorithm for the numerical solution of partial differential equations," *IMA Journal of Applied Mathematics*, vol. 7, no. 2, pp. 216–227, 1971.

[44] B. Vrcej and P. P. Vaidyanathan, "Efficient implementation of all-digital interpolation," *IEEE transactions on image processing*, vol. 10, no. 11, pp. 1639–1646, 2001.

[45] N. S.-N. Lam, "Spatial interpolation methods: a review," *The American Cartographer*, vol. 10, no. 2, pp. 129–150, 1983.

[46] J. W. Demmel, *Applied numerical linear algebra*. Siam, 1997.

[47] Q. I. Rahman and G. Schmeisser, "Characterization of the speed of convergence of the trapezoidal rule," *Numerische Mathematik*, vol. 57, no. 1, pp. 123–138, 1990.

[48] R. A. Diaz and W. J. Herrera, "The positivity and other properties of the matrix of capacitance: Physical and mathematical implications," *Journal of Electrostatics*, vol. 69, no. 6, pp. 587–595, 2011.

[49] W. J. Herrera and R. A. Diaz, "The geometrical nature and some properties of the capacitance coefficients based on laplaces equation," *American Journal of Physics*, vol. 76, no. 1, pp. 55–59, 2008.

[50] J. B. Kruskal, "On the shortest spanning subtree of a graph and the traveling salesman problem," *Proceedings of the American Mathematical society*, vol. 7, no. 1, pp. 48–50, 1956.

[51] D. Aldous and J. M. Steele, "Asymptotics for euclidean minimal spanning trees on random points," *Probability Theory and Related Fields*, vol. 92, no. 2, pp. 247–258, 1992.

[52] R. E. Horton, "Erosional development of streams and their drainage basins; hydrophysical approach to quantitative morphology," *Geological society of America bulletin*, vol. 56, no. 3, pp. 275–370, 1945.

[53] A. N. Strahler, "Quantitative analysis of watershed geomorphology," *Eos, Transactions American Geophysical Union*, vol. 38, no. 6, pp. 913–920, 1957.

[54] J. Smart, "Statistical properties of stream lengths," *Water Resources Research*, vol. 4, no. 5, pp. 1001–1014, 1968.